Precambrian Research 260 (2015) 55–75

Contents lists available at ScienceDirect

Precambrian Research

journal homepage: www.elsevier.com/locate/precamres

Temperature–time evolution of the Assynt Terrane of the Lewisian Gneiss Complex of Northwest Scotland from zircon U-Pb dating and Ti thermometry

John M. MacDonald[a,*], Kathryn M. Goodenough[b], John Wheeler[a], Quentin Crowley[c], Simon L. Harley[d], Elisabetta Mariani[a], Daniel Tatham[a]

[a] School of Environmental Sciences, Jane Herdman Laboratories, University of Liverpool, L69 3GP, UK
[b] British Geological Survey, Murchison House, West Mains Road, Edinburgh, EH9 3LA, UK
[c] Department of Geology, School of Natural Sciences, Trinity College, Dublin 2, Ireland
[d] School of GeoSciences, University of Edinburgh, Edinburgh, EH9 3JW, UK

ARTICLE INFO

Article history:
Received 28 October 2014
Received in revised form 8 January 2015
Accepted 21 January 2015
Available online 31 January 2015

Keywords:
Lewisian Gneiss Complex
Assynt Terrane
Zircon
U-Th-Pb
Ti-in-zircon thermometry

ABSTRACT

The Lewisian Gneiss Complex of Northwest Scotland is a classic Precambrian basement gneiss complex. The Lewisian is divided into a number of terranes on the basis of structural, metamorphic and geochronological evidence. The most well-studied of these is the Assynt Terrane, which forms the central part of the Lewisian outcrop on the Scottish mainland. Field evidence shows that it has a complex tectonothermal history, the early stages of which remain poorly constrained. This paper sets out to better understand the chronology and thermal evolution of the Assynt Terrane through zircon U-Pb dating and Ti-in-zircon thermometry, the latter applied to the Lewisian for the first time. This is placed in context by integration with detailed field mapping, sample petrography, zircon cathodoluminescence (CL) imaging and rare earth element (REE) analysis.

Zircons from six tonalite-trondhjemite-granodiorite (TTG) gneiss samples and two metasedimentary gneiss samples were analysed. The TTG gneisses were predominantly retrogressed to amphibolite-facies; zircons showed a range of CL zoning patterns and REE profiles were similar to those expected for magmatic zircon grains. Zircons from the metasedimentary gneisses also displayed a range of CL zoning patterns and are depleted relative to chondrite in heavy REEs due to the presence of garnet.

Zircon analysis records a spread of concordant U-Pb ages from ~2500 to 3000 Ma. There is no evident correlation of ages with location in the crystal or with CL zoning pattern. A weighted average of $^{207}Pb/^{206}Pb$ ages from the oldest igneous zircon cores from the TTG gneiss samples gives an age of 2958 ± 7 Ma, interpreted to be a magmatic protolith crystallisation age. A weighted average of $^{207}Pb/^{206}Pb$ ages of the youngest metamorphic rims yields an age of 2482 ± 6 Ma, interpreted to represent the last high-grade metamorphism to affect these rocks. Ti-in-zircon thermometry records minimum temperatures of 710–834 °C, interpreted to reflect magmatic crystallisation.

REE profiling enabled the zircons in the metasedimentary rocks to be linked to the presence of metamorphic garnet, but resetting of U-Pb systematics precluded the determination of either protolith or metamorphic ages. Zircons from the metasedimentary gneisses generally record higher minimum temperatures (803–847 °C) than the TTG gneisses, interpreted to record zircon crystallisation in an unknown protolith.

1. Introduction

The Lewisian Gneiss Complex of Northwest Scotland (Fig. 1a) is a classic example of a basement gneiss complex and is an important location for understanding the processes of metamorphism and deformation in lower crustal rocks. Field relationships and metamorphic mineral assemblages allowed Peach et al. (1907)

* Corresponding author. Current address: Department of Earth Sciences and Engineering, Imperial College London, SW7 2AZ, UK. Tel.: +44 02075947326.
E-mail address: john.macdonald@imperial.ac.uk (J.M. MacDonald).

http://dx.doi.org/10.1016/j.precamres.2015.01.009

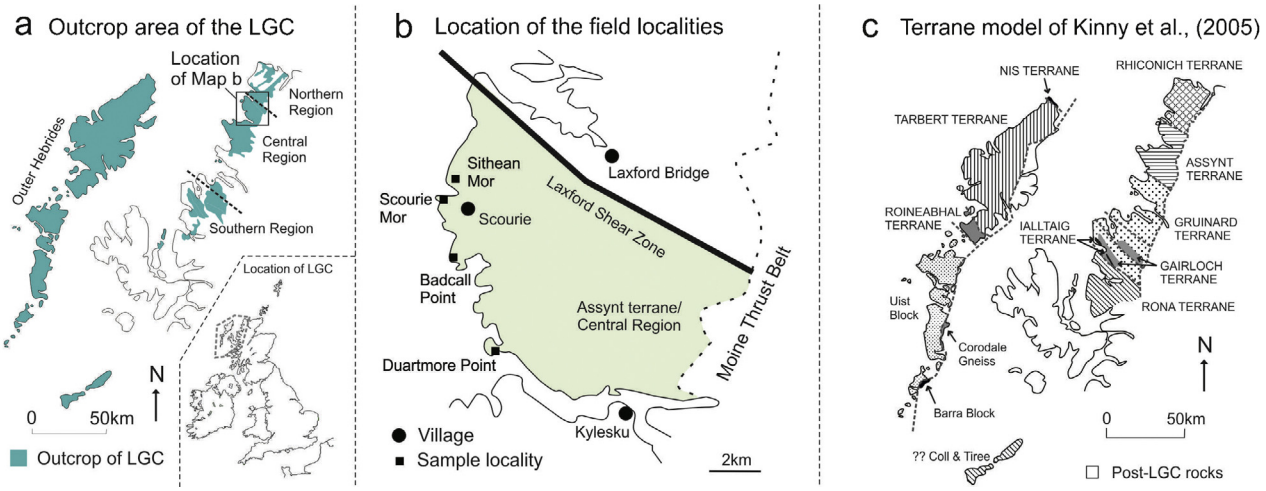

Fig. 1. (a) Location of the outcrop area of the Lewisian Gneiss Complex in Northwest Scotland, inset map shows location in the British Isles; mainland outcrop regions are after Peach et al. (1907). (b) Localities where zircons analysed in this study were taken from. (c) The terrane model of Kinny et al. (2005) showing the different terranes interpreted to make up the Lewisian.

and Sutton and Watson (1951) to determine a relative chronology of tectonothermal events in the Lewisian, providing a framework for the large number of geochemical and geochronological investigations that have been carried out since then (summarised in Kinny et al., 2005; Wheeler et al., 2010; Goodenough et al., 2013). The dominant lithologies in the Lewisian Gneiss Complex are tonalite-trondhjemite-granodiorite (TTG) gneisses, with subordinate mafic and ultramafic gneisses and rare metasedimentary rocks (e.g. Sutton and Watson, 1951; Davies, 1974; Tarney and Weaver, 1987; Johnson and White, 2011; Zirkler et al., 2012). In the area around the village of Scourie (Fig. 1b), three major sets of structures and associated metamorphic assemblages have been recognised in the TTG gneisses and attributed to three tectonothermal events. Sutton and Watson (1951) used the heterogeneous preservation of these structures and assemblages to subdivide the mainland outcrop of the LGC into three regions (Fig. 1a). The area around Scourie was termed the Central Region, bounded to the north and south by the Northern and Southern Regions.

In parts of the Central Region, such as around Scourie, field evidence for all three tectonothermal events is preserved. The earliest event is expressed as strong gneissic layering, which represents the gneissification of the TTG magmatic protoliths. In areas with little subsequent deformation, granulite-facies metamorphic assemblages are preserved, and this metamorphic event is named the Badcallian (Park, 1970). The Badcallian event is also characterised by ultra-high temperatures and partial melting (Johnson et al., 2012, 2013; Rollinson, 2012; Rollinson and Gravestock, 2012). Field evidence for partial melting is clearest in the mafic gneisses where bands of felsic melt permeate these bodies (Johnson et al., 2012, 2013). Geochemical evidence for partial melting comes from whole rock and mineral trace element patterns of TTG and mafic gneisses. Rollinson and Gravestock (2012) determined that light Rare Earth Element (REE) enrichment in clinopyroxenes in mafic gneisses could not be a primary magmatic feature and must have been generated by interaction with a felsic partial melt. Rollinson (2012) built on these partial melting studies to show that the Lewisian TTG protoliths were generated from a LILE- and HFSE-depleted basaltic source.

The subsequent Inverian event is characterised by an amphibolite-facies hydrous static retrogression of dry Badcallian granulite-facies assemblages and localised shear zones up to a few kilometres wide (e.g. Canisp (Evans, 1965; Jensen, 1984; Attfield, 1987)). The Inverian event was followed by the intrusion of the mafic Scourie Dyke Swarm, an important chronological marker. Heterogeneous deformation of the dykes enabled recognition of pre- and post-dyke tectonothermal events. Post-dyke, deformation associated with the Laxfordian amphibolite-facies event heterogeneously overprinted earlier assemblages and structures (Sutton and Watson, 1951). Around Scourie, the Laxfordian event is represented by discrete shear zones a few metres wide, and by widespread static overprinting of earlier granulite-facies assemblages. In the Northern and Southern regions, the Laxfordian deformation and metamorphism is generally more pervasive. The terms Badcallian, Inverian and Laxfordian are used here to refer to the structures and mineral assemblages and the tectonothermal activity they represent; the attributes of each are summarised in Table 1.

As well as the dominant TTG gneisses, parts of the Lewisian Gneiss Complex, including areas around Scourie, contain typically garnetiferous brown-weathering, mica-rich rocks interpreted to be sedimentary in origin (Beach, 1973; Davies, 1974; Okeke et al., 1983; Goodenough et al., 2013). The relationship of these metasedimentary rocks to the rest of the TTG gneisses is not wholly clear. They tend to be spatially associated with mafic and ultramafic gneisses, interpreted to represent an ocean floor supracrustal package (e.g. Davies, 1974; Cartwright et al., 1985; Cartwright and Barnicoat, 1987). Based on structural relationships, Davies (1974) suggested that the mafic–ultramafic and metasedimentary assemblage was juxtaposed against the TTG gneisses prior to the Badcallian tectonothermal event. In support of this, detailed petrographic analysis by Zirkler et al. (2012) indicated partial melting of the metasedimentary rocks in the Badcallian. However, Rollinson and Gravestock (2012) interpreted that due to their dispersed nature within the TTG gneisses, the mafic and ultramafic gneisses, and hence the associated metasedimentary rocks, were intruded by the TTG gneisses and represent the oldest assemblage in the area. Additionally, Friend and Kinny (1995) obtained a magmatic crystallisation age of ~2960 Ma from a TTG gneiss sample which cross-cuts a mafic–ultramafic body at Scourie; hence the mafic–ultramafic and metasedimentary assemblages pre-date crystallisation of the TTG protoliths.

Early workers such as Peach et al. (1907) and Sutton and Watson (1951) assumed that the LGC was one block of crust of a single age and the three tectonothermal events had concurrently affected each of the three regions. Radiometric dating was initially applied with the aim of attributing precise ages to protolith formation and tectonothermal events. However, a large suite of high spatial

Table 1
Summary of the structures and mineral assemblages that characterise the Badcallian, Inverian and Laxfordian tectonothermal events in the Scourie area.

Name	Characteristics
Badcallian	Pyroxene-bearing granulite-facies mineral assemblage, gneissification of TTG protoliths and formation of generally flat-lying gneissic layering, generally no lineation
Inverian	Steeply-dipping kilometre-wide shear zones with amphibolite-facies planar and linear fabrics
Laxfordian	Discrete shear zones, steeply-dipping and several metres wide with amphibolite-facies planar and linear fabrics, static retrogression of pyroxene to hornblende

resolution ion microprobe U-Pb zircon dating from across the LGC has illustrated the complexity of its history, and led to a new interpretation of its formation and tectonothermal evolution (Friend and Kinny, 1995, 2001; Kinny and Friend, 1997; Love et al., 2004, 2010; Kinny et al., 2005). Significant debate continues over the link between radiometric dates and events that can be recognised in the field.

The ages of the younger, Palaeoproterozoic events are generally agreed. Davies and Heaman (2014) dated the main Scourie Dyke Swarm intrusion episode at ~2418–2375 Ma while Corfu et al. (1994) and Kinny and Friend (1997) attributed U-Pb titanite ages of ~1750 Ma to the Laxfordian event. However, dating of protoliths and the pre-Scourie Dyke metamorphic events has proved more controversial. Corfu et al. (1994) obtained U-Pb zircon ages of ~2710 Ma> and ~2490 Ma from gneisses near Badcall Point (Fig. 1b) which they attributed to the Badcallian and Inverian respectively. Subsequently, U-Pb zircon ages from the Central Region led Friend and Kinny (1995) to suggest a magmatic protolith age for the LGC of 2960–3030 Ma with a major metamorphic event at ~2490 Ma; they did not find a significant age cluster at ~2710 Ma. This led them to interpret that the granulite-facies Badcallian event actually occurred at ~2490 Ma with the Inverian occurring soon after but not recorded in the zircons.

Following this, magmatic protolith ages of 2680–2840 Ma were obtained from the Northern Region, with no record of metamorphism at ~2490 Ma (Kinny and Friend, 1997). The difference in age profile for magmatic protolith formation and subsequent tectonothermal activity led to the conclusion that the Northern Region and Central Region were separate crustal blocks. Friend and Kinny (2001) found that different parts of the Outer Hebrides also had different magmatic protolith formation and tectonothermal activity ages. Similarly, Love et al. (2004) found different ages for magmatic protoliths and tectonothermal activity in the southern part of the Central Region. These findings were formalised into a model of discrete terranes with different magmatic protolith ages and tectonothermal histories, which then accreted during or before the Laxfordian event (Kinny et al., 2005) (Fig. 1c). Further work by Love et al. (2010) indicated that the Southern Region was also composed of multiple terranes with varying histories. The Central Region around Scourie was re-named the Assynt Terrane, and the Northern Region the Rhiconich Terrane (Fig. 1c) (Kinny et al., 2005). However, Crowley et al. (2014) was able to distinguish temporally precise ages of both ~2500 Ma and ~2700 Ma from the Assynt Terrane using an innovative CA_ID_TIMS approach. Goodenough et al. (2010) investigated field relationships in the Laxford Shear Zone (Fig. 1a), the boundary between the Assynt and Rhiconich Terranes, and suggested that the two terranes were accreted during the Inverian event at ~2480 Ma (Goodenough et al., 2013).

There have been many previous studies attempting to constrain the thermal history of the Assynt Terrane. Early work used ion exchange geothermometers such as garnet-pyroxene in mafic and ultramafic gneisses, and determined peak metamorphic conditions in the Badcallian between 600 °C and >1000 °C (O'Hara and Yarwood, 1978; Barnicoat, 1983; Sills and Rollinson, 1987). Sills (1983) suggested Inverian retrogression occurred at ~600 °C based on a range of ion exchange thermometers and tentatively estimated >500 °C for Laxfordian metamorphism from muscovites in shear zones. Droop et al. (1999) estimated ~530–630 °C for peak Laxfordian metamorphism from metapelites from the Loch Maree Group in the Southern Region of the Lewisian Gneiss Complex.

More recent attempts to constrain thermal conditions in the Assynt Terrane have involved mineral equilibria modelling. Johnson and White (2011) constructed pseudosections in THERMOCALC (Holland and Powell, 1998) for the bulk composition of a metagabbro and a metapyroxenite from near Scourie. They calculated peak metamorphic temperatures for the Badcallian of 875–975 °C. Zirkler et al. (2012) followed a similar approach in combining mineral equilibria modelling with petrographic observation to determine peak Badcallian metamorphic temperatures of >900 °C from metasedimentary rocks at Stoer, also in the Assynt Terrane. Petrographic characterisation of the metasediments by Zirkler et al. (2012) showed that there was hydrous retrogression of the peak granulite-facies assemblage, evidenced by retrograde growth of hornblende, biotite and other hydrous minerals. This retrogressive assemblage indicated temperatures of 520–550 °C, interpreted to reflect the Inverian tectonothermal event.

Understanding the formation and tectonothermal evolution of the Lewisian Gneiss Complex continues to present challenges. There is ongoing debate into whether the Badcallian tectonothermal event occurred at ~2500 Ma or ~2700 Ma. Crowley et al. (2014) have interpreted both ages to represent high-grade metamorphism from their CA-ID-TIMS measurements but which of these ages relates to the granulite-facies mineral assemblage and structures observed in the field remains debated (Friend and Kinny, 1995; Kinny et al., 2005; Park, 2005; Park et al., 2005; Whitehouse and Kemp, 2010; Goodenough et al., 2013; Crowley et al., 2014). In this contribution, we conduct zircon U-Pb dating and Ti-in-zircon thermometry, the latter applied to the Lewisian for the first time, to investigate the chronology and thermal evolution of the Assynt Terrane. This is placed in context by integration with detailed field mapping, sample petrography, zircon cathodoluminescence (CL) imaging and rare earth element (REE) analysis.

2. Sample characterisation

Zircon grains were collected from eight samples, six from the TTG gneisses which dominate the Assynt Terrane, and two from metasedimentary rocks. The samples of TTG gneiss were collected at two localities that were mapped in detail, Badcall Point and Duartmore Point (Figs. 1b and 2a and b). These samples were chosen to reflect the tectonothermal history of the Assynt Terrane. At Badcall Point, Badcallian gneissic layering is the dominant structure but the Badcallian granulite-facies metamorphic assemblage has been retrogressed, as is typical across much of the Assynt Terrane. Sieve-textured hornblende and quartz have replaced pyroxenes; plagioclase is the other main mineral. Sample JM09/BP02 was taken from this lithology. The Badcallian gneissic layering is rotated and intensified in a ~0.5 m-wide zone which is interpreted to be Inverian in age. Sample JM09/BP01 was taken from within this zone. The Inverian and Badcallian fabrics are cross-cut by an intrusion of the Scourie Dyke Swarm which is in turn cross-cut and deformed by a ~10 m wide Laxfordian shear zone from which samples JM09/BP06 and JM09/BP04 were taken. Both samples have moderate to strong planar and linear fabrics (Fig. 2a) and an

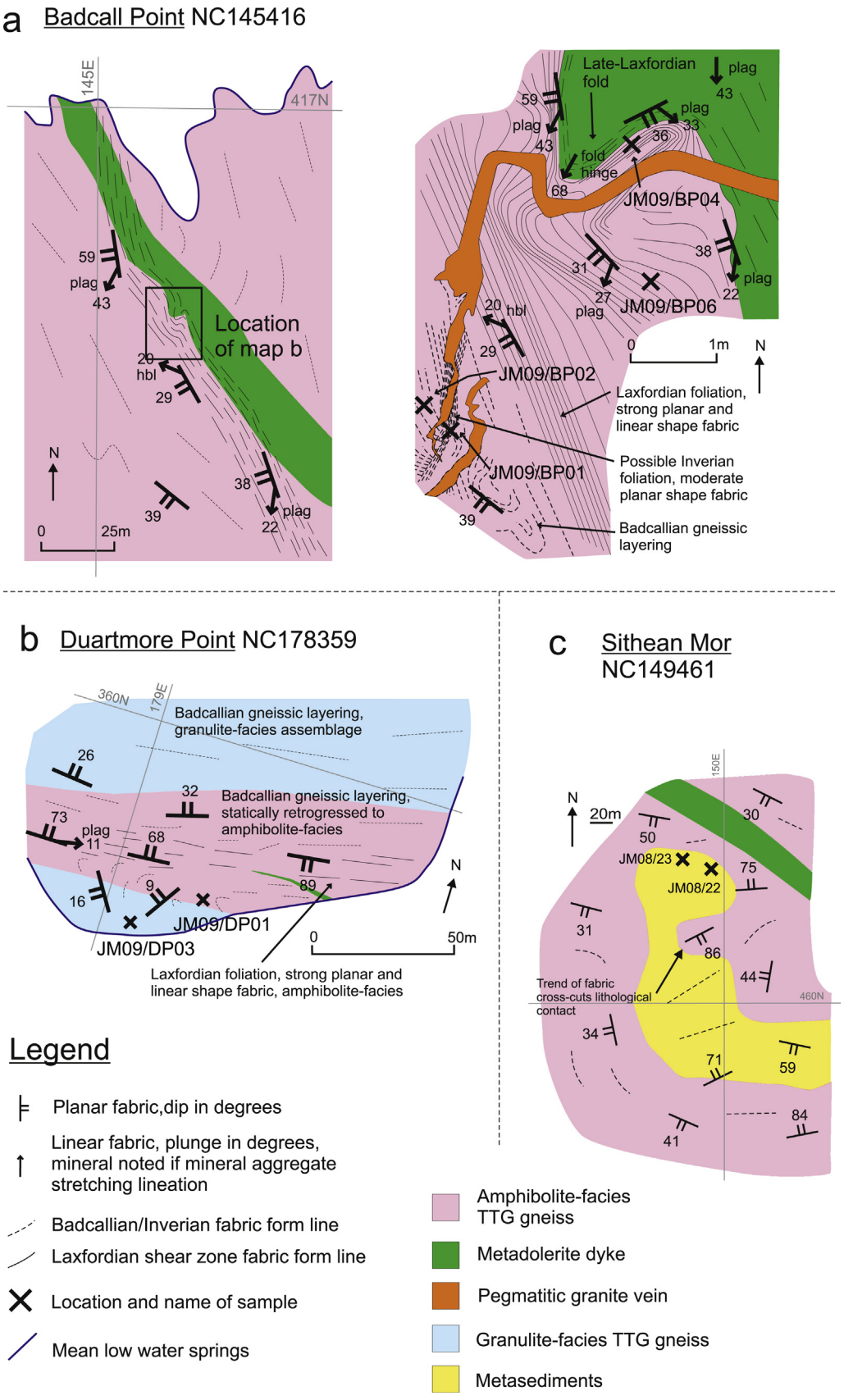

Fig. 2. Field maps showing structures, mineral assemblages and sample localities: (a) Badcall Point, with context map (left) and detail map (right); (b) Duartmore Point; (c) Sithean Mor.

amphibolite-facies hornblende + plagioclase + quartz assemblage. At Duartmore Point (Fig. 2b), the Badcallian layered gneiss retains granulite-facies clinopyroxene but orthopyroxene has largely been replaced by epidote and biotite; plagioclase and quartz are the other major minerals. Sample JM09/DP03 was taken from this lithology. The Badcallian gneissic layering is cross-cut by an intrusion of the Scourie Dyke Swarm which is in turn cross-cut and deformed by a ~15 m wide Laxfordian shear zone. The shear zone has moderate to strong planar and linear fabrics and an amphibolite-facies hornblende + plagioclase + quartz assemblage. On either side of the shear zone is a zone where granulite-facies gneissic layering is preserved but has been statically retrogressed to amphibolite-facies. Sample JM09/DP01 was taken from this zone.

Two samples were taken from the body of metasedimentary rocks at Sithean Mor (Figs. 1b and 2c). The metasedimentary package is internally heterogeneous with biotite- and garnet-rich zones, and more quartzose areas. The biotite- and garnet-rich zones are interpreted to be relict muddy sediments. These grade into the more quartzose zones that by association are interpreted to be relict quartz-rich sediments. This is in agreement with the interpretations of Okeke et al. (1983) and Beach (1973). This outcrop of metasedimentary rocks is surrounded by TTG gneisses with Badcallian gneissic layering. The strike of the layering runs into the metasedimentary outcrop and continues in the form of a moderately-developed planar fabric comprising biotite-rich and biotite-poor layers. Sample JM08/22 has a garnet + biotite + plagioclase + quartz assemblage. The garnet is highly fractured and partially replaced with biotite and quartz. Sample JM08/23 is composed of: lensoid- or arcuate-shaped quartz aggregates, 2–5 mm long and composed of equant 0.5 mm-diameter crystals, possibly porphyroclasts; large partially sericitised plagioclase crystals, possibly also porphyroclasts; a very fine matrix of quartz, feldspar and muscovite; and very high relief kyanite. The kyanite is variably acicular or equant in shape when viewed in thin section, with the different shapes representing different sections through the crystals.

In addition to the zircon-bearing samples, a further sample (JM09/SM09) was taken from Scourie Mor (Fig. 1b) at NC 14146 44175. This sample is representative of the pristine granulite-facies Badcallian assemblage, not seen at the Duartmore Point or Badcall Point localities. It has a granoblastic texture with orthopyroxene, clinopyroxene, plagioclase, quartz and accessory rutile, but does not contain zircon.

3. Zircon analysis

3.1. Analytical methods

Zircons were labelled according to the sample name, followed by "Z" and the zircon number. A prefix of "GM" indicates a zircon on a grain mount; the absence of this prefix indicates a zircon on a thin or thick section. "Ch" before the zircon number indicates a zircon from a thick section. For example, GMBP04Z6 is zircon 6 from sample JM09/BP04 and was on a grain mount; BP06ChZ1 denotes zircon 1 from the thick section of sample JM09/BP06.

Internal chemical zoning in zircons was revealed by cathodoluminescence (CL) imaging carried out in a Philips XL30 scanning electron microscope at the University of Liverpool. The zircons were then analysed by ion microprobe at the Edinburgh Ion Microprobe Facility (EIMF) at the University of Edinburgh. U-Pb isotope analysis was conducted using a Cameca IMS 1270 ion microprobe and analytical procedures follow those of Kelly et al. (2008). U/Pb ratios were calibrated against the 91,500 (Wiedenbeck et al., 1995), SL1 (Maas et al., 1992) and Plesovice (Slama et al., 2008) zircon standards. Plesovice was the primary standard and yielded a mean $^{206}Pb/^{238}U$ ratio of 0.05359 ± 0.00023 (MSWD = 2.4; 95% conf.; $^{206}Pb/^{238}U$ age = 340.5 ± 4.8 Ma; n = 62). A common Pb correction was also applied in-house. Common Pb surface contamination was reduced by rastering the sample with the ion microprobe beam immediately prior to isotope measurement and by production of flat-bottom analysis pits through carefully tuned beam conditions. Correction for in situ common Pb was made using measured ^{204}Pb counts above that of the detector background (typically ~0.2–1.5 ppb). In the analyses for this project, measured common Pb was generally in the range of <5 ppb, although occasionally analyses were much higher than this, likely the result of contamination on the sample surface and in exposed cracks; such analyses were discarded. Uncertainties on all isotopic ratios and ages are quoted at the 2σ level. Plots and age calculations have been made using the computer program ISOPLOT (Ludwig, 2003).

Following U-Pb analysis, trace elements (REEs and Ti) were measured using a Cameca 4f ion microprobe, following the analytical procedures of Kelly and Harley (2005). Analytical reproducibility during the analytical session was tested by regular measurement of REEs and Ti in the 91,500 zircon standard (Wiedenbeck et al., 1995) and NIST SRM610 glass standard. The analyses from the 91,500 zircon show an increase in chondrite-normalised values of trivalent REEs as ionic radius decreases from La to Lu, together with large positive Ce anomaly and small negative Eu anomaly. Good agreement is obtained between the SIMS measurements for zircon 91,500 presented here and those of Whitehouse and Platt (2003) and Hoskin (1998) although there is some variation in REE concentrations in the analyses of 91,500, also encountered by Hoskin (1998). For most REEs (particularly the heavier ones), the average analytical error is <10% (2σ) but for some of the lighter REEs which have lower concentrations, it can be significantly higher. This is interpreted to be partly due to a lack of reproducibility from the spectrometer but also to heterogeneity in the 91,500 standard as noted above. Error on Ti is ~10% (2σ). Analytical reproducibility against the NIST SRM610 glass standard was <6% (2σ) for the elements analysed. Raw data were reduced using the JCION6 software written by John Craven at the University of Edinburgh. REE data were chondrite-normalised against the values of McDonough and Sun (1995).

3.2. Zircon cathodoluminescence

When imaged by cathodoluminescence (CL), the population of zircons showed a range of chemical zoning patterns typical of complex zircons from high-grade metamorphic rocks (Fig. 3). Subrounded cores, both CL-bright and CL-dark, are found in many crystals. Some cores have distinctive oscillatory zoning patterns (e.g. GMBP04Z6 and BP06ChZ1 in Fig. 3, both from samples of TTG gneiss in the Laxfordian shear zone at Badcall Point), indicative of growth from a magma (Corfu et al., 2003). Other cores are homogenous in CL response (e.g. DP01Z6 in Fig. 3, from the statically retrogressed shear zone margin TTG gneiss at Duartmore Point) or may show some irregular zoning. Cores are typically surrounded by rims which are usually CL-bright (e.g. GMDP01Z2 and BP06ChZ1 in Fig. 3, from the statically retrogressed shear zone margin TTG gneiss at Duartmore Point and Laxfordian shear zone TTG gneiss at Badcall point, respectively) but may in some cases have medium or low CL response (CL-dark). The rims are generally homogeneous in CL response and are interpreted to have formed during metamorphism (Corfu et al., 2003). This may have been through solid-state recrystallization of pre-existing magmatic zircon (Hoskin and Black, 2000) or through growth during the partial melting which occurred in the Badcallian tectonothermal event (Johnson et al., 2012, 2013; Rollinson, 2012; Rollinson and Gravestock, 2012). Some whole grains do not have any discernible

Table 2
Ion microprobe zircon trace element data (ppm). CL (cathodoluminescence) zoning pattern identifiers: h = homogeneous; ir = irregular; ir (emb) = irregular embayment; r = rim; r (br) = bright rim; r (dr) = dark rim; c (ozp) = oscillatory zoned core; c (bc) = bright core; c (dc) = dark core.

Sample/spot	CL zoning pattern	Ti	Ba	La	Ce	Pr	Nd	Sm	Eu	Gd	Tb	Dy	Ho	Er	Tm	Yb	Lu	Yb/Gd	Eu/Eu*	Ce/Ce*
JM09/BP02																				
GMBP02Z1-1	h	15.4	0.834	0.248	35.8	1.36	2.51	10.96	6.91	42.1	63.0	114.0	181.2	306.1	418.7	548.7	833.5	13.04	0.95	28.18
GMBP02Z1-2	h	15.9	1.109	0.251	34.5	1.25	2.65	12.01	8.34	39.3	63.7	114.0	175.8	292.5	431.7	517.3	821.5	13.16	1.16	28.19
GMBP02Z2-1	ir	17.7	0.741	0.160	25.8	1.10	2.65	8.83	8.16	24.4	41.9	63.8	111.4	167.5	248.7	308.1	498.3	12.64	1.42	22.98
GMBP02Z2-2	ir	16.8	0.614	0.191	26.2	1.31	2.47	9.57	7.97	25.4	42.6	73.6	106.1	169.7	247.1	299.3	463.8	11.79	1.35	21.39
JM09/BP01																				
BP01Z1-1	ir	18.6	0.917	0.313	20.3	1.15	2.21	8.88	6.47	21.2	24.1	30.6	32.4	40.3	43.2	39.7	58.2	1.87	1.18	16.79
GMBP01Z2-1	ir	14.5	0.465	0.420	26.7	1.56	3.53	10.43	7.68	38.0	66.7	121.9	204.1	362.9	511.3	661.6	997.2	17.41	1.10	18.97
JM09/BP06																				
BP06ChZ1-1	r (br)	17.1	0.317	0.303	31.3	1.24	2.64	8.30	8.76	21.1	24.0	35.5	46.0	64.5	84.2	107.8	165.9	5.10	1.62	25.22
BP06ChZ1-2	c (ozp)	14.6	0.352	0.456	46.7	1.57	5.18	20.96	19.17	62.3	104.1	180.1	298.4	515.8	814.1	1177.9	1976.7	18.91	2.10	32.82
BP06ChZ2-1	c (ozp)	15.8	0.987	0.262	25.2	1.06	2.83	21.87	16.19	92.2	168.9	294.1	476.4	755.8	1011.6	1266.6	1750.1	13.73	1.52	21.93
BP06ChZ2-2	c (ozp)	14.5	0.977	3.202	22.3	1.74	3.08	14.79	15.24	58.2	108.7	191.8	318.6	530.7	681.4	893.1	1297.2	15.33	1.78	10.05
BP06ChZ2-3	c (ozp)	18.1	0.699	0.380	31.6	3.98	12.83	57.67	29.24	159.6	263.4	436.6	676.6	1039.9	1337.9	1684.1	2405.9	10.55	1.98	15.15
BP06ChZ2-6	r (dr)	19.4	0.451	1.008	45.1	1.99	4.67	20.35	8.80	60.6	106.7	177.6	287.0	493.5	698.2	878.2	1317.1	14.50	0.98	26.06
BP06ChZ2-7	ir (emb)	12.1	0.804	0.163	14.3	0.61	0.77	5.66	4.45	20.5	40.5	79.7	145.3	243.3	364.2	492.3	826.2	23.97	0.87	16.22
BP06ChZ2-9	r (dr)	17.5	0.808	1.983	69.4	3.62	5.50	19.07	11.54	50.9	83.9	143.5	224.1	364.0	542.8	692.7	1042.1	13.62	1.38	29.33
BP06Z3-1	ir	12.6	0.502	0.649	6.7	0.59	0.29	1.49	3.13	6.2	21.0	70.8	183.1	459.7	850.6	1358.7	2354.3	219.13	1.13	6.05
BP06Z3-2	ir	16.8	0.627	0.493	5.6	0.54	0.34	1.68	3.82	6.3	27.0	95.6	269.1	709.2	1370.3	2042.0	3485.7	322.94	1.35	5.55
BP06Z3-3	ir	10.5	0.485	0.775	34.6	2.02	3.31	12.20	9.47	32.8	47.0	82.4	146.8	329.5	597.0	889.7	1646.8	27.16	1.41	20.74
BP06Z3-4	ir	14.2	0.557	0.093	1.6	0.25	0.13	1.15	1.70	2.1	3.6	11.9	30.9	75.1	125.0	213.2	359.9	100.05	0.94	2.81
BP06Z3-5	ir	14.8	0.354	0.224	5.3	0.67	0.29	2.26	2.81	6.6	15.9	39.4	90.5	189.3	318.7	478.3	783.7	72.02	0.94	5.64
GMBP06Z1-1	r (br)	18.6	0.711	0.473	29.8	1.70	4.34	18.42	9.20	57.7	91.4	148.2	235.4	370.4	497.8	690.1	922.1	11.96	1.05	20.20
GMBP06Z1-2	r (br)	17.8	0.549	0.331	28.6	1.65	2.79	13.86	8.16	40.9	62.5	106.2	159.3	261.6	339.8	444.6	621.5	10.88	1.10	20.34
GMBP06Z1-3	c (bc)	15.6	0.954	0.412	23.3	0.60	2.25	8.85	6.16	44.0	68.5	131.7	213.3	323.4	453.4	580.0	786.1	13.19	0.85	23.23
GMBP06Z2-1	ir (emb)	16.7	0.392	0.280	39.1	1.84	7.05	20.41	13.06	59.6	97.2	168.1	271.7	385.9	507.9	647.3	1094.6	10.86	1.46	26.86
GMBP06Z2-2	c (ozp)	18.7	0.428	0.157	38.7	1.46	5.09	27.35	18.71	113.0	182.7	298.1	456.1	675.5	889.8	1014.7	1678.2	8.98	1.58	30.39
GMBP06Z3-1	r (br)	15.3	0.611	0.295	27.1	0.52	1.65	5.15	4.64	41.5	67.2	121.2	179.0	295.4	375.0	464.3	739.7	11.18	0.68	30.06
GMBP06Z3-2	r (br)	14.8	0.635	0.063	24.4	0.87	1.63	10.50	4.91	36.0	56.8	104.8	155.6	270.3	375.0	393.2	697.6	10.92	0.72	25.30
GMBP06Z3-3	c (dc)	16.3	0.315	0.291	26.8	0.52	3.05	8.84	3.43	47.4	92.9	138.2	235.1	315.9	475.5	529.3	767.8	11.17	0.46	29.70
GMBP06Z4-1	r	15.0	0.885	0.284	30.0	2.04	4.50	24.92	15.07	80.8	127.7	212.8	330.7	514.8	657.8	853.0	1130.7	10.56	1.47	19.68
GMBP06Z4-2	c (bc)	15.7	0.604	0.322	27.1	1.23	3.03	12.24	7.06	38.4	59.3	97.0	151.3	241.4	335.1	441.8	622.5	11.50	0.99	21.73
GMBP06Z4-3	c (bc)	13.7	0.617	0.315	27.1	1.29	3.79	16.51	11.17	50.0	81.8	131.7	206.0	331.2	447.5	548.4	818.4	10.97	1.37	21.38
GMBP06Z4-4	r	14.4	0.606	0.188	29.7	1.94	4.86	23.39	14.24	76.0	128.2	211.3	336.4	508.1	661.0	872.7	1179.0	11.48	1.43	20.33
GMBP06Z5-1	r (br)	15.8	0.316	0.435	25.9	0.40	2.03	9.89	3.15	33.5	61.5	93.8	166.1	276.0	377.1	447.6	773.9	13.38	0.48	28.38
GMBP06Z5-2	c (dc)	14.6	0.450	0.283	43.2	0.72	2.95	12.67	5.72	70.2	111.8	212.4	365.3	565.4	860.9	1101.4	1763.6	15.70	0.63	42.99
GMBP06Z6-1	ir	23.7	0.511	0.246	36.1	1.70	5.50	16.56	8.14	74.7	111.7	199.9	317.9	491.0	653.4	806.6	1222.3	10.80	0.85	25.88
JM09/BP04																				
GMBP04Z1-1	r (br)	17.2	0.206	0.325	38.8	1.03	6.42	15.54	8.33	54.8	84.0	149.4	229.3	368.8	500.3	592.0	934.0	10.80	0.99	33.33
GMBP04Z1-2	r (br)	18.3	0.233	0.178	44.2	1.44	4.77	22.46	12.84	73.8	124.9	210.4	316.4	530.1	697.1	835.8	1320.1	11.33	1.31	34.75
GMBP04Z2-1	r (br)	16.9	0.389	0.178	33.2	0.89	2.14	11.31	7.67	24.8	40.4	57.3	78.2	124.7	200.8	238.4	349.9	9.61	1.28	32.17
GMBP04Z2-2	r (br)	11.8	0.488	0.030	36.9	1.33	2.84	11.89	6.61	40.2	76.2	128.8	198.2	296.2	485.3	576.3	861.0	14.34	0.92	31.66
GMBP04Z3-1	c (bc)	16.1	1.254	1.899	33.1	10.21	22.42	79.01	99.26	166.1	215.9	280.3	380.0	541.0	684.6	814.0	1135.2	4.90	6.34	9.51
GMBP04Z3-2	c (bc)	16.2	1.439	0.353	34.3	1.26	2.66	12.53	7.91	35.9	66.3	110.3	171.4	284.9	382.2	492.9	701.0	13.71	1.14	26.95
GMBP04Z4-1	r (br)	13.8	0.935	0.435	42.7	2.87	7.89	18.80	8.42	43.7	69.8	122.0	190.9	293.5	385.9	488.0	808.8	11.18	1.07	23.50
GMBP04Z4-2	r (br)	14.8	0.166	0.287	42.6	2.51	7.14	14.26	9.27	50.7	76.6	115.7	185.7	239.2	346.7	478.1	781.8	9.43	1.15	25.47
GMBP04Z4-3	c (dc)	8.5	0.148	1.305	32.1	1.88	3.98	6.78	8.18	27.2	47.7	75.3	128.6	204.9	343.2	429.8	697.5	15.80	1.40	17.97
GMBP04Z5-1	h	17.1	0.242	0.338	33.0	1.53	4.85	17.50	8.09	50.3	78.9	142.9	222.3	316.5	466.2	574.6	922.4	11.42	0.98	24.16
GMBP04Z5-2	h	17.3	0.664	0.228	31.8	1.36	5.71	18.21	12.77	57.6	89.8	138.1	247.7	350.5	512.9	533.8	994.8	9.26	1.47	25.22
GMBP04Z6-1	r (br)	18.9	0.243	0.189	30.8	1.35	4.12	12.19	4.90	38.6	74.3	113.8	187.9	278.8	415.1	513.6	820.2	13.30	0.69	24.79
GMBP04Z6-2	c (ozp)	19.1	0.304	0.142	39.9	1.95	5.06	21.07	12.72	65.1	108.7	187.8	304.8	483.1	603.0	781.6	1184.7	12.01	1.37	27.63
GMBP04Z7-1	h	21.0	0.277	0.141	32.3	0.90	2.99	12.50	7.75	33.9	57.4	100.3	151.8	246.0	309.4	440.5	674.4	13.01	1.14	31.64
GMBP04Z7-2	h	18.5	0.007	0.258	32.9	1.15	4.09	15.07	6.57	46.9	67.7	125.7	180.5	273.9	416.6	515.7	824.6	10.99	0.83	27.76
GMBP04Z7-3	h	20.7	0.109	0.186	29.8	1.31	1.90	17.59	4.44	38.2	56.6	102.9	167.1	269.2	391.6	426.6	770.9	11.17	0.59	24.35

GMBP04Z8-2	h	19.1	0.928	0.313	30.5	1.63	3.62	15.61	9.84	48.7	78.5	130.2	201.4	324.5	433.4	526.6	808.3	10.81	1.23	21.86
GMBP04Z8-3	h	16.6	0.828	0.252	32.4	1.62	3.80	15.34	12.65	55.8	88.7	141.1	225.9	341.9	479.5	608.7	866.6	10.91	1.50	23.74
GMBP04Z9-1	h	16.6	0.220	0.196	32.8	1.48	3.53	14.04	7.79	47.8	83.2	124.4	211.3	306.2	437.9	523.9	901.5	10.96	0.99	25.33
GMBP04Z9-2	h	14.8	0.159	0.185	34.2	1.33	3.66	11.61	8.00	38.7	62.9	75.3	126.4	217.4	266.2	324.6	558.0	8.39	1.13	27.79
JM09/DP03																				
GMDP03Z1-1	r (br)	13.0	0.380	0.207	29.0	1.14	2.11	13.05	10.24	43.9	71.8	112.4	192.3	314.7	450.7	607.2	879.2	13.84	1.36	24.97
GMDP03Z1-2	r (br)	12.6	0.601	0.236	24.6	0.91	2.32	9.96	9.25	33.1	52.0	83.7	137.4	222.7	320.4	431.0	645.8	13.03	1.41	23.02
GMDP03Z1-3	c (ozp)	6.7	0.655	0.385	34.2	0.88	3.28	16.41	18.27	62.4	94.4	168.1	267.0	445.9	621.2	818.0	1186.9	13.10	2.06	30.34
GMDP03Z1-4	r (br)	14.0	0.251	0.357	27.0	1.01	2.23	11.11	10.21	34.3	53.2	92.5	145.9	244.3	343.9	459.1	686.6	13.38	1.51	23.14
GMDP03Z1-5	r (br)	13.0	1.335	0.538	28.4	1.99	4.00	16.92	16.06	45.2	71.6	112.6	173.2	294.5	420.4	575.8	874.4	12.73	2.04	17.89
GMDP03Z2-1	c (ozp)	19.6	0.435	0.580	8.3	1.02	1.92	10.59	20.72	49.7	97.4	177.0	311.6	516.6	733.2	1000.7	1492.3	20.15	2.67	6.59
DP03Z2-1	h	19.4	0.698	2.283	32.1	3.98	7.48	16.61	18.49	34.8	41.8	60.4	74.9	123.3	155.4	224.8	303.6	6.46	2.58	12.81
JM09/DP01																				
DP01Z4-1	h	17.7	0.663	0.252	35.5	0.99	2.66	15.05	8.67	55.4	94.5	167.4	257.2	424.1	569.6	724.5	1073.9	13.09	1.03	31.92
DP01Z4-2	h	16.3	0.647	0.334	32.4	0.89	2.25	13.18	7.37	48.7	84.2	145.7	232.1	389.0	510.3	626.4	932.5	12.86	0.94	29.25
DP01Z6-1	r (br)	17.1	1.115	0.577	29.5	1.80	4.10	16.78	12.57	52.5	73.4	117.6	180.9	276.9	364.6	446.3	671.0	8.50	1.51	19.13
DP01Z6-2	r (br)	15.9	0.811	0.348	27.6	1.51	4.11	15.71	12.36	47.4	73.5	114.4	166.5	262.2	363.1	435.0	648.4	9.17	1.55	20.25
DP01Z6-3	c (dc)	15.0	0.584	0.357	31.4	1.03	2.49	9.47	7.09	24.0	32.1	53.1	74.7	101.4	136.6	159.8	253.1	6.65	1.22	26.64
DP01Z6-4	r (br)	17.7	0.529	0.470	26.4	1.82	3.03	14.73	12.85	40.3	60.4	95.1	142.0	220.2	304.1	377.0	547.7	9.36	1.73	17.48
DP01Z6-5	r (br)	18.5	0.581	0.610	26.9	1.53	4.18	16.49	14.28	48.5	72.5	113.8	171.5	252.7	355.0	452.9	624.4	9.34	1.77	18.42
DP01Z10-1	r (br)	20.2	0.908	0.835	32.4	2.10	4.01	15.13	16.79	39.5	62.2	96.9	141.8	219.1	279.8	372.9	540.4	9.43	2.27	18.87
DP01Z10-2	r (br)	19.8	0.613	0.380	25.6	1.35	3.44	13.46	9.75	39.5	59.7	98.3	149.9	221.4	318.8	393.0	565.1	9.95	1.34	19.43
DP01Z10-3	r (br)	15.7	1.028	0.144	24.5	1.20	2.30	11.07	9.49	28.6	44.0	68.7	113.4	168.6	222.3	280.4	403.4	9.79	1.51	21.12
GMDP01Z1-1	r (br)	13.3	0.639	0.286	27.2	0.78	1.18	7.36	4.66	27.7	50.5	82.0	131.7	222.5	341.8	435.8	690.4	15.74	0.79	26.29
GMDP01Z1-2	r (br)	8.3	0.834	0.211	26.6	0.98	1.59	8.07	7.52	23.1	46.2	83.1	135.1	232.3	340.5	467.3	697.6	20.26	1.35	24.40
GMDP01Z2-1	r (br)	14.9	0.338	0.283	20.9	0.89	2.29	10.76	8.53	32.7	51.1	82.1	120.7	186.0	255.7	339.4	475.4	10.39	1.29	19.34
GMDP01Z2-2	c (dc)	14.8	0.649	0.253	25.2	0.90	1.48	5.81	6.28	17.1	30.2	46.9	67.6	111.5	154.2	205.6	304.6	12.00	1.31	23.49
GMDP01Z2-4	c (dc)	14.1	0.539	0.297	28.0	1.08	3.06	16.49	16.55	50.2	69.0	94.2	109.6	130.6	140.8	164.7	181.0	3.28	2.03	23.82
GMDP01Z2-5	r (br)	15.1	0.428	0.284	19.8	1.16	2.10	9.16	7.69	28.5	44.7	72.5	110.4	172.4	245.6	309.4	491.0	10.87	1.25	16.46
GMDP01Z3-1	h	20.7	0.957	0.554	24.7	1.74	3.68	14.71	13.21	46.4	78.7	118.4	184.5	288.7	371.7	478.1	714.3	10.31	1.69	16.33
GMDP01Z4-1	h	9.9	0.532	0.237	27.2	1.58	3.69	12.89	10.67	36.2	54.6	87.6	131.6	198.6	270.3	334.2	463.8	9.24	1.52	20.19
GMDP01Z4-2	h	12.7	0.136	0.497	26.1	1.92	3.51	15.31	12.82	42.6	58.4	93.0	139.5	217.2	293.2	378.8	533.6	8.89	1.68	16.81
GMDP01Z5-1	c (dc)	10.8	0.894	0.469	14.9	0.62	2.04	8.01	9.60	27.9	44.0	72.1	108.1	174.9	241.3	302.8	490.6	10.85	1.60	14.29
GMDP01Z5-2	r (br)	17.2	1.265	0.346	21.1	1.17	2.53	8.11	5.61	22.5	35.5	55.9	84.8	133.3	166.3	222.9	338.4	9.90	1.01	17.08
GMDP01Z6-1	r (br)	13.7	0.755	0.142	24.1	0.72	1.98	9.97	7.38	29.1	50.0	86.0	137.3	218.9	312.2	428.9	599.3	14.74	1.18	25.98
GMDP01Z6-2	r (br)	14.1	0.748	0.262	21.3	0.76	1.55	7.87	8.52	28.6	47.3	80.7	134.9	224.7	321.7	433.8	644.9	15.17	1.41	21.07
GMDP01Z6-3	c (dc)	13.8	0.408	0.293	24.9	0.80	1.88	8.03	8.25	26.4	44.1	71.3	114.2	186.2	272.3	379.4	583.4	14.38	1.41	23.86
GMDP01Z7-1	h	19.3	0.641	0.403	25.0	1.55	3.89	12.37	12.06	40.3	64.8	97.5	148.9	238.0	308.6	391.3	568.7	9.72	1.66	17.89
GMDP01Z8-1	r (br)	15.3	1.410	0.215	24.6	0.73	2.12	11.50	8.74	33.5	59.0	105.2	173.2	280.5	387.5	531.9	846.1	15.86	1.30	25.30
GMDP01Z9-3	ir	13.4	1.287	0.080	25.9	1.05	1.92	10.33	7.30	27.1	42.2	59.2	84.9	124.6	158.8	213.1	293.0	7.87	1.19	24.38
JM08/22																				
GM22Z1-1	c (ozp)	21.3	0.145	0.623	27.8	4.98	16.33	87.52	42.92	230.9	314.3	444.7	583.3	759.4	985.4	1013.3	1667.5	4.39	2.41	11.76
GM22Z1-2	c (bc)	19.9	0.110	0.284	40.2	6.69	19.49	90.32	48.48	245.6	343.9	477.5	619.2	807.7	1041.6	1137.0	1789.9	4.63	2.65	15.22
GM22Z2-1	c (ozp)	22.9	0.063	0.202	5.0	1.51	2.86	19.80	3.19	50.1	44.7	64.2	62.2	60.1	66.1	84.1	94.2	1.68	0.38	3.80
GM22Z3-1	c (ozp)	19.3	0.193	0.277	7.7	1.27	3.56	19.99	15.92	74.3	131.6	199.9	269.7	362.9	452.0	519.5	840.4	6.99	1.64	6.17
GM22Z4-1	ir	19.8	0.156	0.419	19.2	1.01	3.09	17.73	9.63	40.3	61.7	87.5	102.6	132.6	164.6	170.1	204.7	4.22	1.26	16.02
JM08/23																				
GM23Z1-1	ir	17.8	0.872	0.444	28.6	3.82	10.31	48.06	2.85	151.7	212.6	286.9	308.6	330.6	342.1	364.7	428.3	2.40	0.20	13.83
GM23Z2-1	ir	19.5	0.138	0.385	27.9	2.42	6.41	44.56	1.66	136.7	218.9	254.2	303.3	315.9	334.3	365.1	410.7	2.67	0.12	16.65
GM23Z2-2	ir	24.3	0.103	0.573	30.8	3.10	8.75	36.74	5.28	117.5	190.4	284.3	407.7	547.7	696.2	790.7	1063.9	6.73	0.43	16.04
GM23Z4-1	r (br)	24.3	0.098	0.045	11.0	1.77	7.86	25.21	4.49	60.6	58.1	62.5	66.3	62.4	62.5	46.7	69.2	0.77	0.49	8.15
GM23Z4-2	r (br)	25.1	0.263	1.430	14.5	2.80	8.88	28.35	14.41	55.5	58.4	57.7	54.3	50.4	50.1	53.7	61.2	0.97	1.57	7.04
GM23Z5-1	h	20.5	0.340	0.581	30.9	4.52	13.11	26.78	6.80	102.5	167.9	288.0	460.0	693.2	898.2	908.6	1538.6	8.87	0.60	13.68
GM23Z5-2	h	17.9	0.129	0.153	31.1	2.17	7.58	24.43	4.92	78.3	144.6	220.2	362.9	571.1	605.0	844.0	1248.2	10.78	0.49	20.39
GM23Z6-1	ir	26.6	0.028	0.238	25.9	1.71	7.34	28.61	2.58	95.9	143.8	185.8	224.7	244.5	247.9	259.1	321.9	2.70	0.23	18.54
GM23Z6-2	ir	22.0	0.218	0.325	31.8	3.46	9.97	56.00	3.34	162.6	258.4	317.3	346.0	339.0	318.7	306.0	314.9	1.88	0.23	16.33
GM23Z6-3	ir	24.4	0.230	0.395	36.6	3.02	7.98	48.48	6.60	145.6	233.1	353.8	493.6	703.5	871.8	1001.1	1412.0	6.88	0.47	19.80

Table 3
Ion microprobe U-Th-Pb data for zircons analysed in this study. CL zoning pattern identifiers as Table 2.

Sample/spot	CL zoning pattern	U (ppm)	Th (ppm)	Pb (ppm)	Th/U	$^{204}Pb_c$ (ppb)	$^{207}Pb/^{206}Pb$	2σ	$^{207}Pb/^{235}U$	2σ	$^{206}Pb/^{238}U$	2σ	Error Corr.	% Disc.	$^{207}Pb/^{206}Pb$ age	2σ
JM09/BP02																
GMBP02Z1-1	h	33.10	82.63	27.88	2.56	4.49	0.188	0.006	13.332	0.587	0.514	0.017	0.732	1.86	2725	48
GMBP02Z1-2	h	33.55	85.05	31.31	2.60	1.66	0.205	0.005	15.957	0.644	0.564	0.018	0.791	-0.50	2868	40
GMBP02Z2-1	ir	51.03	59.13	32.96	1.19	1.06	0.179	0.003	12.224	0.360	0.495	0.012	0.857	1.98	2644	26
GMBP02Z2-2	ir	49.84	61.14	33.11	1.26	1.44	0.182	0.004	12.579	0.441	0.502	0.014	0.805	1.71	2668	34
JM09/BP01																
BP01Z1-1	ir	47.98	26.41	26.43	0.56	2.61	0.169	0.003	11.200	0.331	0.480	0.012	0.854	0.85	2549	26
BP01Z1-2	ir	44.44	23.85	24.32	0.55	1.13	0.172	0.004	11.339	0.369	0.477	0.011	0.731	2.58	2581	36
GMBP01Z2-1	ir	171.81	272.79	113.48	1.63	2.30	0.167	0.002	10.839	0.285	0.471	0.012	0.931	1.49	2526	16
JM09/BP06																
BP06ChZ1-1	r (br)	49.48	38.36	27.89	0.80	2.48	0.170	0.003	10.953	0.333	0.468	0.012	0.810	3.09	2554	30
BP06ChZ1-2	c (ozp)	421.30	294.94	299.81	0.72	0.00	0.217	0.001	17.415	0.365	0.583	0.012	0.977	-0.12	2956	8
BP06ChZ2-1	c (ozp)	72.76	66.12	54.21	0.93	2.57	0.219	0.003	17.668	0.500	0.585	0.014	0.850	0.12	2973	24
BP06ChZ2-4	r (dr)	165.93	101.29	101.28	0.63	6.75	0.190	0.003	13.543	0.366	0.518	0.012	0.846	1.79	2739	24
BP06ChZ2-5	ir (emb)	35.73	30.51	24.17	0.88	1.61	0.195	0.008	14.633	0.831	0.545	0.020	0.655	-0.82	2782	68
BP06ChZ2-7	ir (emb)	29.38	49.56	24.71	1.73	4.38	0.197	0.005	15.864	0.646	0.584	0.018	0.771	-5.76	2802	42
BP06ChZ2-8	c (ozp)	151.28	156.14	110.55	1.06	3.53	0.204	0.002	15.925	0.387	0.566	0.012	0.877	-1.12	2859	18
BP06Z3-1	ir	88.81	4.38	50.43	0.05	2.22	0.195	0.002	14.604	0.375	0.543	0.013	0.934	-0.31	2786	14
BP06Z3-2	ir	24.46	3.43	15.87	0.14	0.73	0.223	0.008	18.255	0.910	0.594	0.019	0.653	-0.10	3002	60
BP06Z3-3	ir	23.45	9.87	13.17	0.43	5.10	0.179	0.008	12.310	0.631	0.500	0.014	0.542	1.04	2640	70
BP06Z3-4	ir	2.61	0.99	1.39	0.39	0.77	0.169	0.009	11.213	0.796	0.480	0.022	0.637	0.98	2552	90
BP06Z3-5	ir	209.28	8.36	124.24	0.04	2.45	0.208	0.002	16.112	0.398	0.563	0.012	0.886	0.31	2887	18
GMBP06Z1-2	r (br)	20.42	20.19	12.79	1.01	1.00	0.182	0.003	12.399	0.456	0.495	0.016	0.858	2.87	2668	32
GMBP06Z2-1	ir (emb)	24.40	31.31	15.62	1.32	1.51	0.167	0.003	11.107	0.360	0.483	0.013	0.820	-0.54	2526	30
GMBP06Z2-2	c (ozp)	30.23	39.97	22.13	1.36	0.12	0.189	0.004	14.106	0.514	0.543	0.015	0.757	-2.38	2729	40
GMBP06Z3-1	r (br)	18.00	12.48	10.42	0.71	0.00	0.174	0.004	11.699	0.477	0.488	0.015	0.778	1.29	2595	42
GMBP06Z3-2	r (br)	21.50	12.85	11.81	0.61	2.73	0.163	0.003	10.688	0.329	0.476	0.012	0.808	-1.01	2485	30
GMBP06Z4-1	r	32.61	39.32	22.51	1.24	2.37	0.203	0.007	14.444	0.640	0.517	0.014	0.621	5.65	2847	56
GMBP06Z4-2	c (bc)	19.40	20.18	12.59	1.07	1.62	0.179	0.007	12.560	0.636	0.509	0.015	0.573	-0.34	2643	68
GMBP06Z4-3	c (bc)	19.78	20.79	12.78	1.08	1.22	0.180	0.008	12.520	0.684	0.505	0.017	0.624	0.53	2650	70
GMBP06Z4-4	r	22.60	22.98	12.94	1.04	8.06	0.153	0.004	9.690	0.351	0.458	0.011	0.670	-1.96	2384	46
GMBP06Z5-1	r (br)	12.79	7.76	6.94	0.62	2.48	0.170	0.004	10.923	0.467	0.467	0.016	0.785	3.14	2552	44
GMBP06Z5-2	c (dc)	52.42	111.53	41.06	2.18	1.21	0.186	0.006	12.960	0.532	0.506	0.013	0.609	2.29	2703	54
GMBP06Z6-1	ir	37.75	40.14	25.22	1.09	1.49	0.219	0.006	15.330	0.592	0.508	0.015	0.741	10.90	2972	42
JM09/BP04																
GMBP04Z1-1	r (br)	35.34	48.52	24.83	1.41	5.24	0.189	0.006	13.421	0.576	0.515	0.015	0.669	2.08	2734	52
GMBP04Z1-2	r (br)	35.24	49.49	27.80	1.44	4.20	0.213	0.005	16.677	0.565	0.568	0.015	0.776	0.90	2927	34
GMBP04Z2-1	r (br)	23.51	24.05	13.66	1.05	6.27	0.167	0.005	10.594	0.434	0.460	0.012	0.628	3.54	2528	54
GMBP04Z2-2	r (br)	35.08	32.98	20.40	0.96	1.47	0.168	0.003	10.807	0.326	0.468	0.010	0.742	2.33	2533	34
GMBP04Z3-1	c (bc)	16.46	21.09	10.03	1.31	0.49	0.173	0.007	10.886	0.583	0.457	0.015	0.615	6.02	2583	70
GMBP04Z3-2	c (bc)	21.05	25.57	13.85	1.25	3.94	0.173	0.005	11.932	0.450	0.501	0.013	0.709	-1.41	2583	44
GMBP04Z4-1	r (br)	23.11	29.88	13.83	1.33	0.10	0.168	0.004	10.430	0.364	0.449	0.011	0.702	5.89	2541	42
GMBP04Z4-2	r (br)	21.63	26.78	13.27	1.27	2.43	0.160	0.004	10.352	0.366	0.468	0.011	0.650	-0.66	2459	46
GMBP04Z4-3	c (dc)	127.60	55.92	66.72	0.45	4.59	0.163	0.001	10.516	0.239	0.469	0.010	0.948	0.10	2482	12
GMBP04Z5-1	h	20.13	24.51	15.47	1.25	1.53	0.201	0.008	15.977	0.997	0.577	0.027	0.738	-3.69	2832	68
GMBP04Z5-2	h	28.26	24.28	18.60	0.88	1.17	0.190	0.008	13.890	0.750	0.531	0.016	0.572	-0.32	2738	72
GMBP04Z6-1	r (br)	15.38	14.35	9.58	0.96	0.76	0.179	0.007	12.277	0.625	0.499	0.016	0.623	1.24	2640	64
GMBP04Z6-2	c (ozp)	34.99	49.14	28.31	1.44	1.73	0.211	0.009	16.985	0.888	0.584	0.019	0.634	-1.83	2912	64
GMBP04Z7-1	h	18.32	19.41	10.71	1.09	1.69	0.167	0.004	10.582	0.431	0.459	0.014	0.753	3.61	2528	44
GMBP04Z7-2	h	12.54	9.88	7.24	0.81	2.17	0.164	0.003	10.849	0.362	0.481	0.012	0.775	-1.45	2494	34
GMBP04Z7-3	h	16.48	18.01	10.64	1.12	4.32	0.167	0.005	11.649	0.536	0.505	0.018	0.791	-4.19	2530	46
GMBP04Z7-4	h	30.80	41.16	21.78	1.37	2.11	0.191	0.005	13.705	0.512	0.521	0.014	0.720	1.54	2747	42
GMBP04Z8-2	h	13.39	8.05	7.78	0.62	2.27	0.206	0.009	13.864	0.861	0.487	0.021	0.680	11.02	2876	74

GMBP04Z8-3	h	28.76	20.31	16.61	0.72	1.92	0.179	0.006	11.960	0.511	0.484	0.013	0.615	3.94	2647	54
GMBP04Z9-1	h	21.87	29.00	16.12	1.36	3.31	0.188	0.007	14.128	0.900	0.546	0.028	0.799	-3.33	2720	62
GMBP04Z9-2	h	30.11	20.81	17.56	0.71	3.67	0.185	0.010	12.413	0.829	0.488	0.018	0.546	4.93	2694	90
JM09/DP03																
GMDP03Z1-1	r (br)	65.61	52.17	42.71	0.82	2.19	0.188	0.002	13.819	0.379	0.533	0.013	0.881	-1.04	2725	22
GMDP03Z1-2	r (br)	42.13	28.79	26.59	0.70	6.27	0.189	0.003	13.758	0.448	0.528	0.015	0.859	0.00	2733	28
GMDP03Z1-3	c (ozp)	82.66	71.55	47.02	0.89	1.82	0.162	0.001	10.409	0.255	0.466	0.011	0.959	0.29	2475	12
GMDP03Z1-4	r (br)	34.50	24.66	21.87	0.73	1.97	0.194	0.006	14.015	0.578	0.525	0.015	0.700	1.85	2772	48
GMDP03Z2-1	c (ozp)	33.96	12.58	21.94	0.38	0.93	0.219	0.010	17.060	0.974	0.564	0.019	0.599	3.00	2974	74
DP03Z2-1	h	439.84	358.71	257.43	0.84	4.50	0.178	0.002	11.763	0.303	0.480	0.011	0.926	4.09	2633	16
JM09/DP01																
DP01Z4-1	h	15.29	2.24	7.41	0.15	0.00	0.166	0.004	10.629	0.369	0.463	0.013	0.788	2.74	2522	36
DP01Z4-2	h	14.04	2.12	7.69	0.16	0.75	0.188	0.006	13.338	0.541	0.514	0.014	0.664	1.82	2725	48
DP01Z6-1	r (br)	18.27	11.02	9.64	0.62	0.35	0.169	0.003	10.605	0.390	0.454	0.014	0.866	5.39	2551	30
DP01Z6-2	r (br)	17.20	8.79	9.14	0.52	0.59	0.166	0.004	10.734	0.417	0.468	0.014	0.793	1.83	2521	38
DP01Z6-3	c (dc)	57.95	87.23	36.86	1.54	0.32	0.166	0.004	10.556	0.359	0.460	0.012	0.780	3.21	2521	36
DP01Z6-4	r (br)	14.72	9.57	8.34	0.67	0.00	0.177	0.005	11.725	0.515	0.480	0.015	0.733	3.67	2625	50
DP01Z6-5	r (br)	18.57	8.94	9.75	0.49	1.25	0.171	0.004	10.911	0.407	0.463	0.014	0.797	4.30	2565	36
DP01Z10-1	r (br)	13.87	5.02	7.16	0.37	1.67	0.178	0.007	11.415	0.536	0.465	0.014	0.625	6.53	2634	60
DP01Z10-2	r (br)	14.54	5.07	7.79	0.36	0.79	0.184	0.008	12.208	0.677	0.482	0.015	0.574	5.50	2685	74
DP01Z10-3	r (br)	15.54	6.57	7.58	0.43	4.85	0.158	0.004	9.575	0.368	0.441	0.012	0.725	3.14	2430	44
DP01Z10-4	c (dc)	39.05	35.39	22.26	0.93	5.30	0.182	0.004	11.457	0.439	0.457	0.014	0.803	9.16	2670	38
GMDP01Z1-1	r (br)	36.48	20.76	19.37	0.58	1.29	0.167	0.002	10.596	0.298	0.461	0.011	0.885	3.05	2523	22
GMDP01Z1-2	r (br)	27.15	10.41	14.10	0.39	1.14	0.164	0.003	10.677	0.341	0.471	0.012	0.800	0.59	2502	32
GMDP01Z2-1	r (br)	15.09	11.70	12.08	0.80	0.00	0.225	0.008	19.960	1.007	0.643	0.023	0.715	-6.12	3017	56
GMDP01Z2-2	c (dc)	89.07	105.38	53.54	1.21	2.28	0.163	0.001	10.372	0.264	0.463	0.011	0.942	1.23	2482	14
GMDP01Z2-4	c (dc)	149.86	173.21	103.04	1.19	2.17	0.192	0.002	13.849	0.360	0.524	0.013	0.952	1.59	2758	12
GMDP01Z2-5	r (br)	21.17	8.45	12.12	0.41	0.26	0.187	0.006	13.130	0.580	0.509	0.016	0.710	2.42	2717	52
GMDP01Z3-1	h	15.12	7.08	8.83	0.48	0.72	0.194	0.010	13.629	0.898	0.508	0.020	0.594	4.71	2780	86
GMDP01Z4-1	h	14.84	7.77	7.87	0.54	1.52	0.164	0.003	10.532	0.381	0.467	0.015	0.876	1.01	2494	28
GMDP01Z4-2	h	12.34	6.70	6.89	0.56	0.96	0.165	0.004	11.116	0.482	0.489	0.017	0.782	-2.41	2506	44
GMDP01Z5-1	c (dc)	81.03	33.84	50.53	0.43	5.62	0.198	0.002	14.929	0.398	0.548	0.013	0.916	-0.44	2805	18
GMDP01Z5-2	r (br)	11.57	6.02	6.12	0.53	0.30	0.168	0.004	10.783	0.389	0.464	0.011	0.673	3.29	2542	44
GMDP01Z6-1	r (br)	5.41	3.20	3.31	0.61	1.08	0.203	0.009	14.440	0.822	0.516	0.019	0.651	5.83	2849	70
GMDP01Z6-2	r (br)	24.23	19.41	16.76	0.82	1.15	0.200	0.003	15.491	0.506	0.561	0.016	0.882	-1.60	2827	24
GMDP01Z6-3	c (dc)	65.70	61.02	45.59	0.95	2.38	0.201	0.003	15.229	0.475	0.549	0.016	0.916	0.58	2836	20
GMDP01Z7-1	h	14.67	7.37	8.24	0.52	0.98	0.177	0.008	12.006	1.237	0.492	0.045	0.887	1.71	2624	78
GMDP01Z8-1	r (br)	19.81	13.34	11.37	0.69	0.86	0.184	0.007	12.209	0.578	0.482	0.012	0.542	5.59	2686	66
GMDP01Z9-3	ir	58.50	27.94	30.01	0.49	1.33	0.164	0.002	10.285	0.281	0.456	0.011	0.898	2.88	2493	20
JM08/22																
GM22Z1-1	c (ozp)	98.42	112.96	72.56	1.18	0.00	0.206	0.004	15.870	0.521	0.558	0.014	0.781	0.63	2876	34
GM22Z1-2	c (bc)	152.83	181.19	111.25	1.22	0.94	0.200	0.003	15.121	0.389	0.549	0.012	0.835	0.05	2823	24
GM22Z2-1	c (ozp)	172.11	246.58	96.22	1.47	6.30	0.165	0.002	9.292	0.240	0.409	0.010	0.903	11.84	2506	18
GM22Z3-1	c (ozp)	409.93	185.31	225.64	0.46	0.74	0.173	0.002	11.660	0.271	0.489	0.010	0.908	0.86	2587	16
JM08/23																
GM23Z2-1	ir	110.41	78.14	66.20	0.73	1.14	0.177	0.004	12.247	0.367	0.503	0.011	0.746	-0.27	2620	34
GM23Z2-2	ir	78.76	69.45	47.04	0.90	0.70	0.177	0.003	11.807	0.323	0.483	0.011	0.797	3.27	2627	26
GM23Z4-1	r (br)	138.07	290.26	108.04	2.16	1.57	0.182	0.003	12.754	0.350	0.509	0.011	0.811	0.58	2668	26
GM23Z4-2	r (br)	136.05	233.58	103.19	1.76	2.65	0.188	0.003	13.602	0.387	0.524	0.012	0.784	0.33	2726	28
GM23Z5-1	h	74.92	73.40	50.93	1.01	0.30	0.196	0.005	14.420	0.504	0.534	0.013	0.698	1.23	2792	40
GM23Z5-2	h	61.85	57.41	40.43	0.95	1.99	0.186	0.004	13.405	0.443	0.522	0.014	0.784	0.15	2710	34
GM23Z6-2	ir	144.50	87.46	85.49	0.62	4.87	0.174	0.003	12.187	0.385	0.508	0.012	0.778	-2.08	2595	34
GM23Z6-3	ir	88.35	88.90	60.25	1.03	1.43	0.194	0.004	14.276	0.480	0.533	0.014	0.759	0.75	2777	34

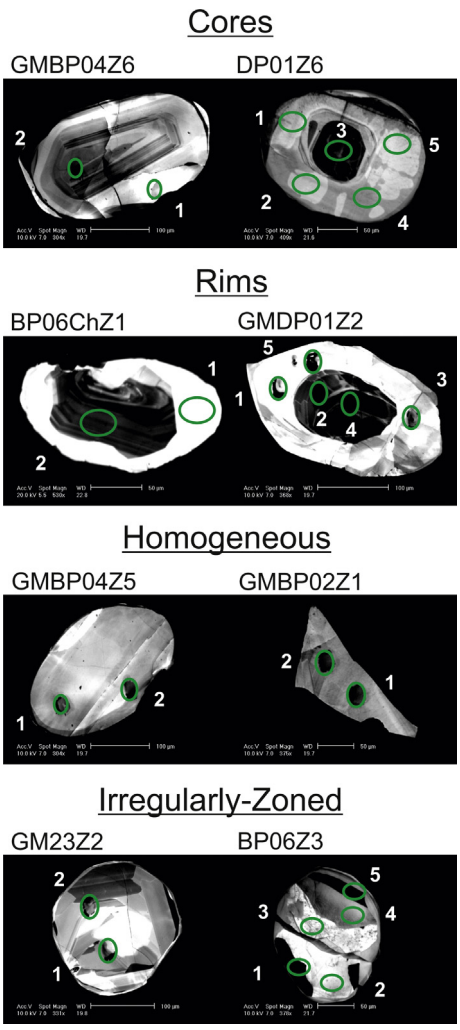

Fig. 3. Representative images showing the four cathodoluminescence (CL) categories of zircons from the population analysed in this study, with crystal names and ion microprobe spot numbers annotated.

internal zoning patterns – these are termed homogeneous (e.g. GMBP04Z5 and GMBP02Z1 in Fig. 3, from the Laxfordian shear zone TTG gneiss sample and statically retrogressed TTG gneiss samples, respectively, both from Badcall Point), although it cannot be ruled out that they contain distinct zones beneath the level of polishing. A number of crystals are irregular in their CL zoning pattern – they have no recognisable core or rim structures and cannot be clearly assigned to any particular formation mechanism (e.g. GM23Z2 and BP06Z3 in Fig. 3, from a metasedimentary gneiss sample from Sithean Mor and a Laxfordian shear zone TTG gneiss sample at Badcall Point, respectively). For the purposes of analysing zircon U-Pb and Ti to gain further insight into the temperature-time history of the Assynt Terrane, the CL zoning patterns were divided into four groups: cores (oscillatory-zoned, homogeneous or heterogeneous zoning, CL-bright or CL-dark); rims (CL-bright or CL-dark); homogeneous zircons; and irregular zonation. Zircons from each sample have a range of zoning patterns (Tables 2 and 3).

3.3. Zircon rare earth elements

Rare earth element (REE) profiling of zircons was carried out as it can link distinct CL domains to metamorphic assemblages in the host rock, therefore giving a better constraint to petrogenetic information recorded by zircon (e.g. Whitehouse and Kamber, 2003; Kelly and Harley, 2005).

103 spot analyses of REE were made, covering all zircon CL zonation types (Table 2). The majority of zircon analyses from Badcall Point and Duartmore Point show a typical magmatic zircon REE profile of increasing chondrite-normalised La-Lu with a positive Ce anomaly and a negative Eu anomaly (Fig. 4a–d). Yb/Gd ratio (an easy way of assessing the relative concentrations of heavy REEs to middle REEs) is generally 8–15 (Table 2). There is no clear distinction in REE profile between the different CL zoning pattern categories (Fig. 4b and d). A few analyses from both localities deviate from the typical pattern. Four analyses from an irregularly-zoned zircon from sample JM09/BP06, from the Laxfordian shear zone at Badcall Point, are relatively depleted in light and middle REEs and have very high Yb/Gd ratios of 72–323 (Fig. 4a and d). A single analysis from an irregularly-zoned zircon from sample JM09/BP01 (Inverian zone, Badcall point), in the Inverian shear zone at Badcall Point, has a flat heavy REE profile (Yb/Gd = 1.87) (Fig. 4a and b) while one core analysis from statically retrogressed sample JM09/DP01 at Duartmore Point also has a relatively flat heavy REE profile (Yb/Gd = 3.28) (Fig. 4b and e).

Most zircon REE profiles from the metasedimentary rocks at Sithean Mor (samples JM08/22 and JM08/23) have relatively flat REE profiles: all bar 2 of the 15 analyses have Yb/Gd of <7 (Table 2, Fig. 4c and f). The highest two Yb/Gd values are from a homogeneous zircon while the two analyses from zircon rims have Yb/Gd of <1. Zircon cores and irregularly-zoned zircons have a range of Yb/Gd values of ~1–7 (Table 2, Fig. 4c and f). There is no clear correlation between Yb/Gd ratio and CL zoning pattern as rims, irregularly-zoned crystals and a core analysis all have Yb/Gd ratio of <3.

3.4. Zircon U-Th-Pb

In order to investigate the chronological history of the Assynt Terrane, a total of 103 U-Th-Pb spot analyses were conducted on the same analytical spots as the REE profiles. U contents range from 2 to 440 ppm while Th ranges from 1 to 360 ppm, although the majority of analyses are 10–100 ppm for both Th and U (Table 3). There is a wide range in Th and U contents within each sample although zircons from the metasedimentary rocks from Sithean Mor (samples JM08/22 and JM08/23) cluster towards the top of the range for Th and U (Fig. 5a; Table 3). There is no correlation between CL zoning pattern and Th or U contents; each of the four zoning pattern types records a wide range in Th and U (Fig. 5b; Table 3). Th/U is generally in the range 0.5–2, although some analyses from an irregularly-zoned zircon from sample JM09/BP06 (TTG gneiss in Laxfordian shear zone, Badcall Point) are as low as 0.04 (Fig. 5a and b; Table 3).

As well as a range in Th and U concentrations, there is also a range in $^{207}Pb/^{206}Pb$ ages from 2384 ± 46 Ma to 3017 ± 56 Ma across all the analysed zircons (Table 3). It would be expected that zircon cores record the oldest ages and rims record younger ages but in fact there is no such relationship in this population. Age, U content and Th/U do not correlate with sample history nor CL zoning pattern (Fig. 5c–f; Table 3). Each sample records a range of $^{207}Pb/^{206}Pb$ ages as do the different CL zoning patterns (Fig. 6a and b). The ages are mainly concordant (−2% to +5%) although some are more discordant (Table 3) and the data define a spread along concordia with no obvious clustering representing protolith or metamorphic ages (Fig. 6c and d).

3.5. Zircon Ti

Ti contents of zircons were measured along with U-Th-Pb and REEs so that Ti-in-zircon thermometry (Watson and Harrison,

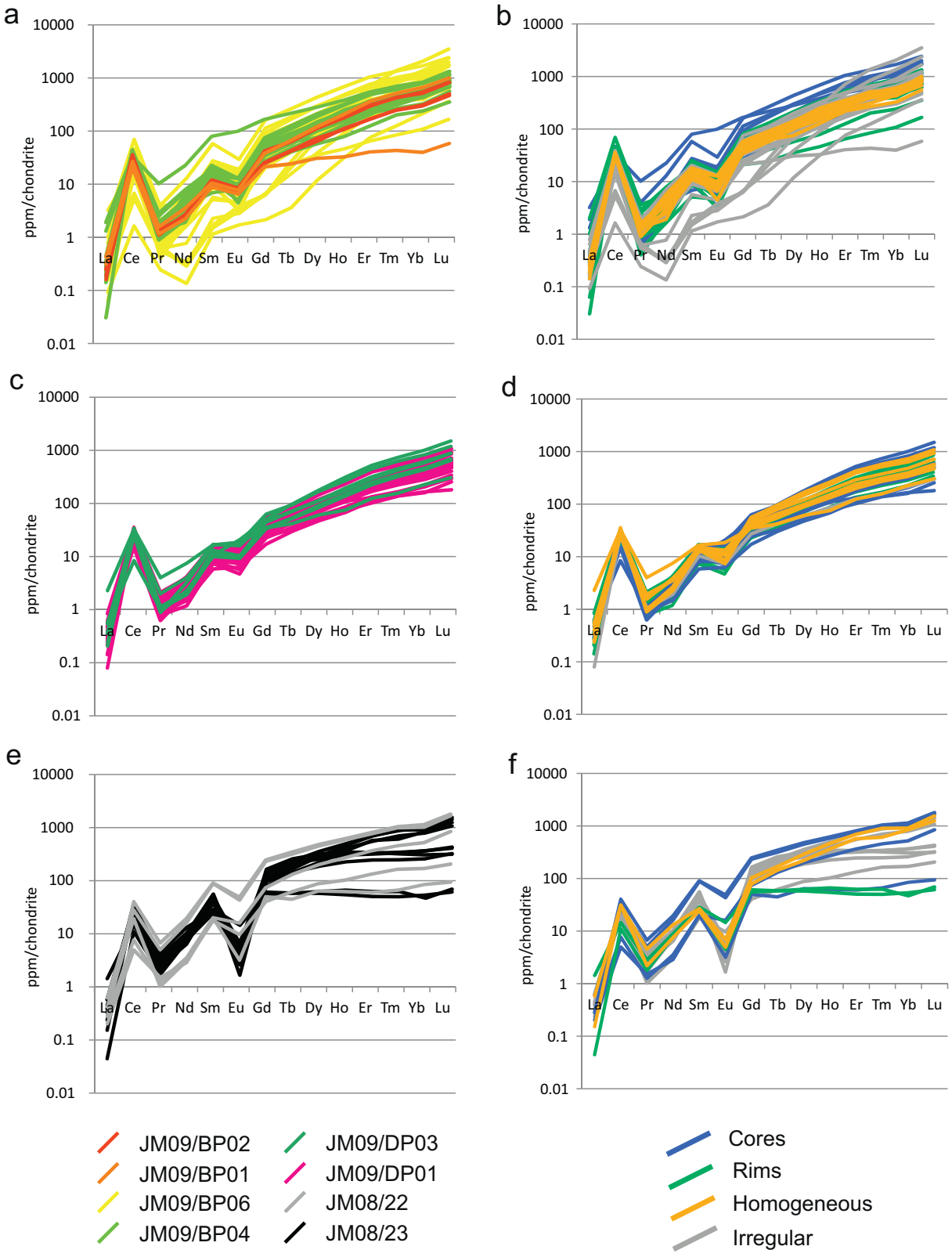

Fig. 4. Matsuda plots of zircon rare earth element profiles for: (a) Badcall Point colour-coded by sample; (b) Badcall Point colour-coded by cathodoluminescence zoning pattern; (c) Duartmore Point colour-coded by sample; (d) Duartmore Point colour-coded by cathodoluminescence zoning pattern; (e) Sithean Mor colour-coded by sample; (f) Sithean Mor colour-coded by cathodoluminescence zoning pattern; values normalised against chondrite values of McDonough and Sun (1995). (For interpretation of the references to colour in this figure legend, the reader is referred to the web version of the article.)

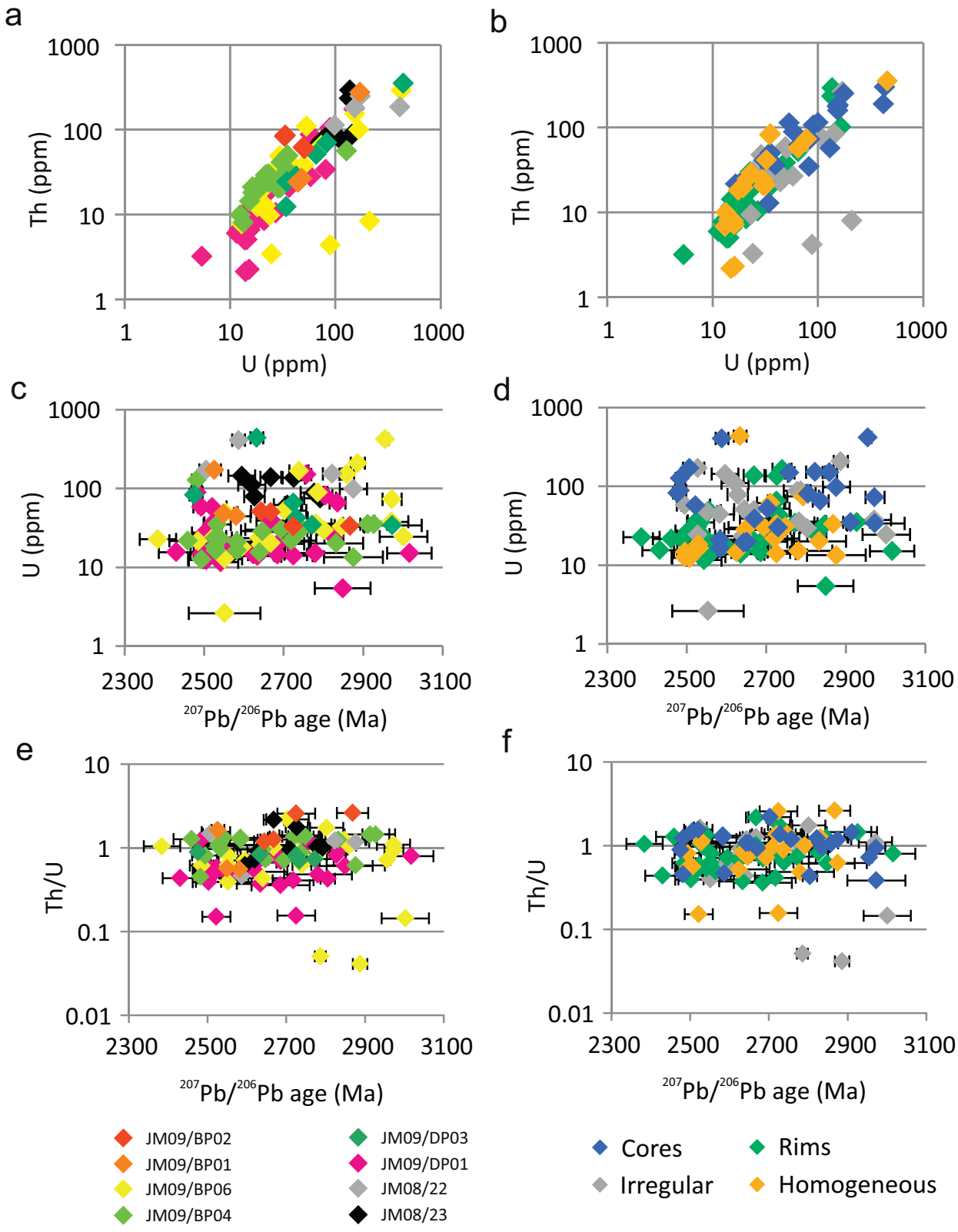

Fig. 5. U-Th-Pb chemistry of zircons from this study plotted as: Th concentration (ppm) vs. U concentration (ppm) colour-coded by sample (a) and by cathodoluminescence zoning pattern (b); U concentration (ppm) vs. ^{207}Pb/^{206}Pb age colour-coded by sample (c) and by cathodoluminescence zoning pattern (d); Th/U ratio vs. ^{207}Pb/^{206}Pb age colour-coded by sample (e) and by cathodoluminescence zoning pattern (f). (For interpretation of the references to colour in this figure legend, the reader is referred to the web version of the article.)

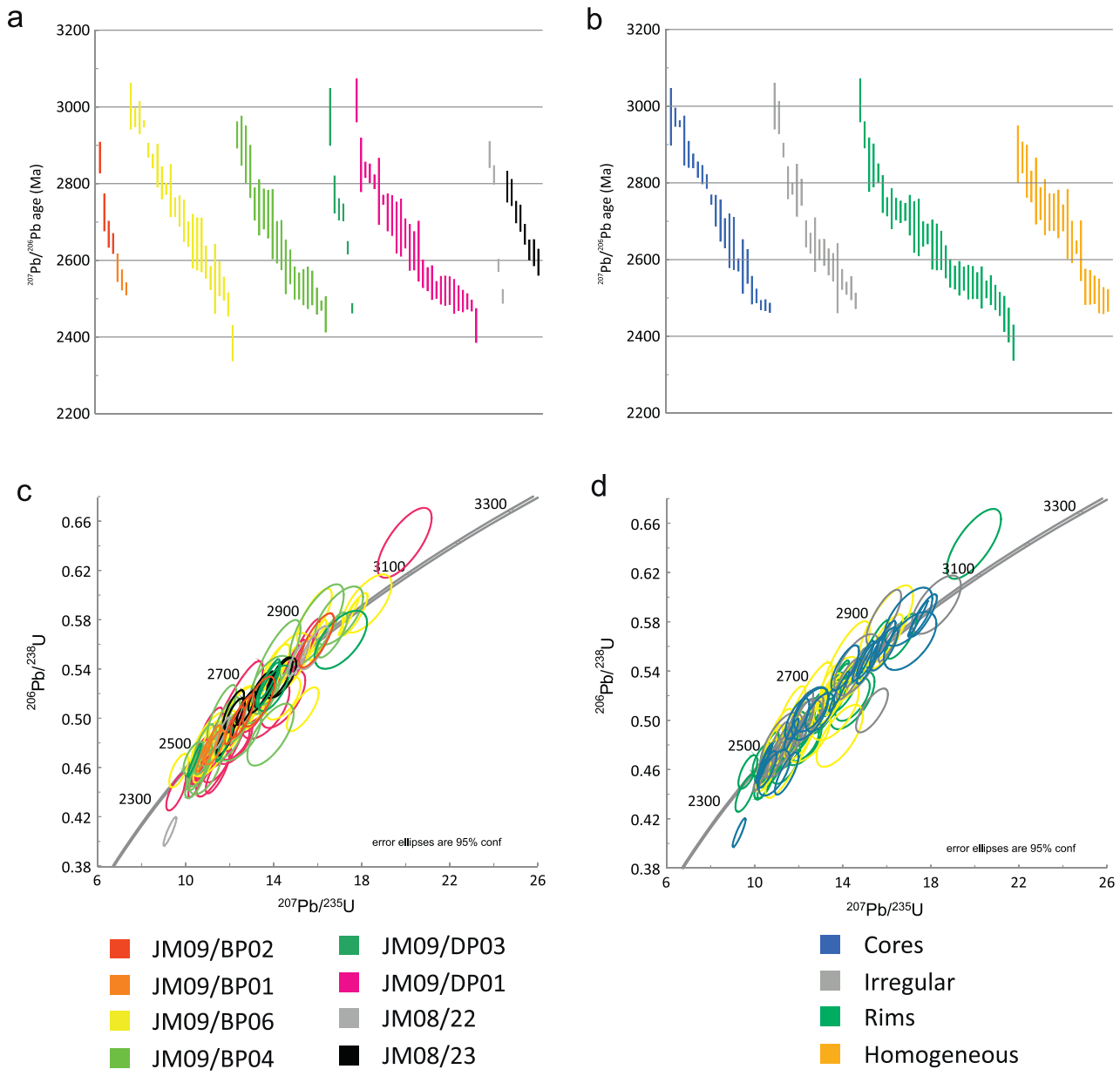

Fig. 6. Spread of ^{207}Pb/^{206}Pb ages recorded by zircons in this study: (a) ^{207}Pb/^{206}Pb ages with 2σ errors colour-coded by sample; (b) ^{207}Pb/^{206}Pb ages with 2σ errors colour-coded by cathodoluminescence zoning pattern; (c) Wetherill concordia plot of zircon Pb/U ratios colour-coded by sample; (d) Wetherill concordia plot of zircon Pb/U ratios colour-coded by cathodoluminescence zoning pattern. (For interpretation of the references to colour in this figure legend, the reader is referred to the web version of the article.)

2005; Watson et al., 2006) could be applied for the first time to further the understanding of the temperature history of the Assynt Terrane. The abundance of Ti in zircon in equilibrium with rutile and quartz is proportional to temperature and therefore provides a crystallisation thermometer for the zircon and its host rock. It was hypothesised that the Ti thermometer would record the magmatic protolith crystallisation temperatures and/or the temperature of the Badcallian or Inverian metamorphism. Ti contents ranged from 6 to 27 ppm (Table 2). Zircons from metasedimentary samples from Sithean Mor had higher average Ti concentrations than Badcall Point and Duartmore Point although there was no clear distinction between the two samples from this locality (Fig. 7a). Zircons from Duartmore Point and Badcall Point had a similar range of Ti concentrations and again there was no clear distinction between samples with different tectonothermal histories at each locality. There was also no clear correlation between CL zoning pattern category and Ti content (Fig. 7b), nor between Ti content and ^{207}Pb/^{206}Pb age (Fig. 7c and d). Some intragranular variation in Ti content was observed (e.g. between core and rim in zircon GMDP03Z1, granulite-facies TTG gneiss, Duartmore Point) and also intradomain variation (e.g. in the core of zircon BP06ChZ2, TTG gneiss in Laxfordian shear zone, Badcall Point) but these variations were minor and restricted to a small number of grains (Table 2).

4. Discussion

4.1. REE patterns

The relative abundance of the different REE in zircon has been shown to vary according to the environment in which the zircon formed or was modified (e.g. Bea et al., 1994; Rubatto, 2002; Whitehouse and Kamber, 2003; Rubatto and Hermann, 2006). For

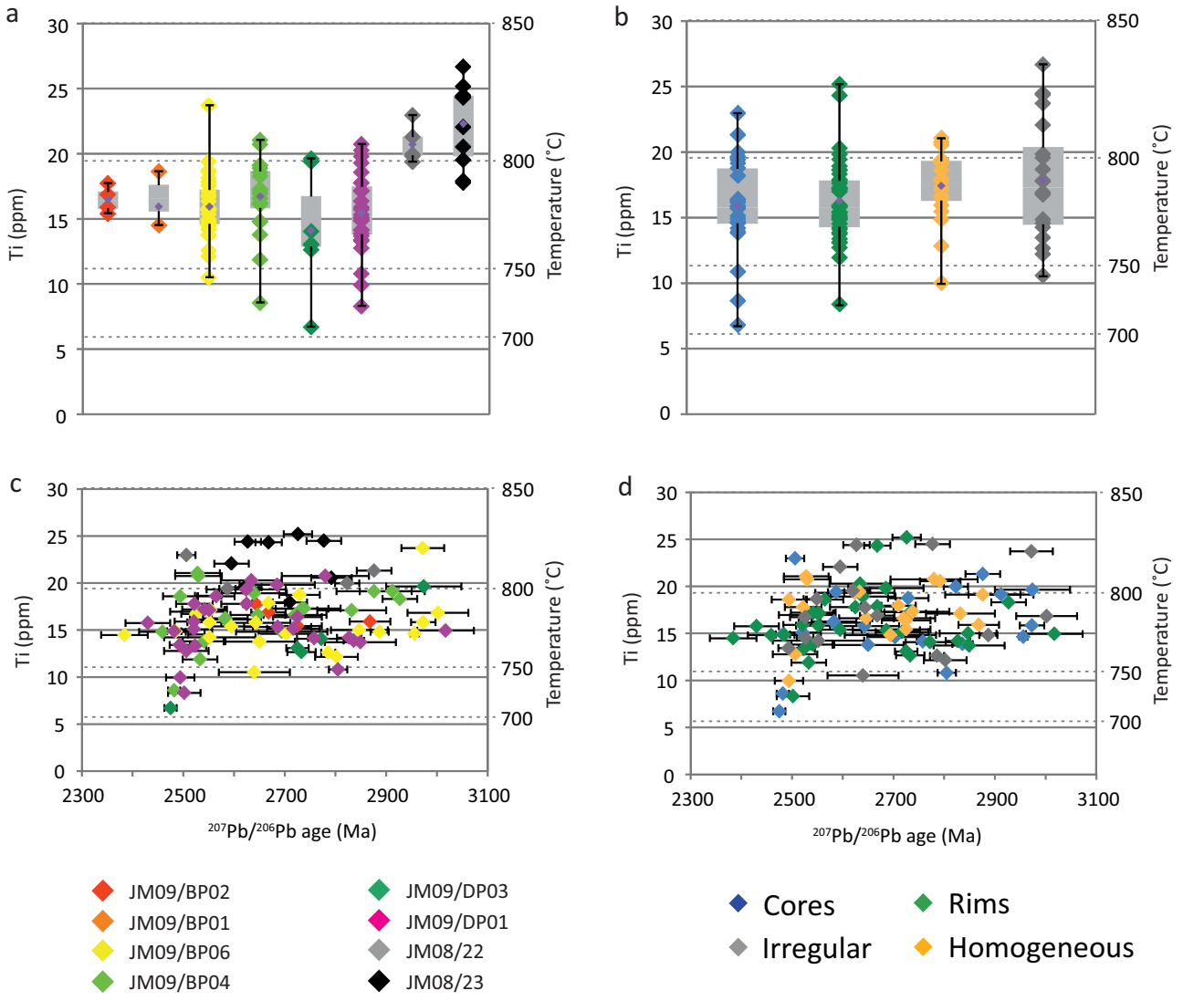

Fig. 7. Ti content (ppm) and Ti-in-zircon temperature (at $a_{TiO_2} = 1$) of zircons in this study: (a) Box-and-whiskers plot of Ti content colour-coded by sample showing mean (small diamond), 50% quartile (shaded box) and 75% quartile (whiskers); (b) Box-and-whiskers plot of Ti content as in (a) but colour-coded by cathodoluminescence zoning pattern; (c) Ti content plotted against ^{207}Pb/^{206}Pb ages colour-coded by sample; (d) Ti content plotted against ^{207}Pb/^{206}Pb ages colour-coded by cathodoluminescence zoning pattern. (For interpretation of the references to colour in this figure legend, the reader is referred to the web version of the article.)

example, zircon grown from a felsic-intermediate magma typically has a steeply HREE-enriched chondrite-normalised La-Lu profile due to a preference for the smaller ionic radius heavier REEs over the larger lighter REEs (Murali et al., 1983; Hinton and Upton, 1991; Hoskin and Ireland, 2000; Whitehouse and Kamber, 2003) but with a positive Ce anomaly (Ce/Ce*) and negative Eu anomaly (Eu/Eu*). Zircon formed or modified during metamorphism, however, may deviate from this pattern (e.g. Kelly and Harley, 2005). The REE composition of zircon that grows or is modified during metamorphism will be affected by concurrent growth or resorption of other REE-sequestering minerals such as garnet, which preferentially incorporates heavy REEs (Rubatto, 2002; Whitehouse and Platt, 2003), monazite, which contains light REEs (Bea and Montero, 1999; Schaltegger et al., 1999; Rubatto et al., 2001), or amphibole, which incorporates middle REEs (Davidson et al., 2007). Rollinson and Gravestock (2012) showed that some clinopyroxenes in Lewisian pyroxenites exerted a strong influence in light REEs while orthopyroxene preferentially incorporated heavy REEs.

In the TTG gneisses, zircon Yb/Gd ratios are generally 8–15 (Table 2) which is lower than that measured by Kelly and Harley (2005) for magmatic zircon (Yb/Gd = 20–30). The lack of variation in REE profile between the different CL zoning pattern categories (Fig. 4b and d) suggests that zircon did not exchange REEs with metamorphic minerals such as garnet and monazite, which strongly influence the REE profile in zircon, even if they were present in the rocks. Analyses which deviate from the typical pattern may have been influenced by the presence of other minerals. The four analyses from an irregularly-zoned zircon from sample JM09/BP06, from the Laxfordian shear zone at Badcall Point, are relatively depleted in light and middle REEs and have very high Yb/Gd ratios of 72–323 (Fig. 4a and d). Monazite sequesters light REEs (Bea and Montero, 1999) but monazite has not been recorded in the TTG gneisses of the LGC. Amphibole sequesters middle REEs (Davidson et al., 2007) but amphibole is abundant in the TTG gneisses in the Inverian and Laxfordian assemblages and does not appear to have had a similar effect on the REE pattern of any of the other zircon grains analysed from this shear zone sample.

The analyses with the flat heavy REE profiles (an irregularly-zoned zircon from sample JM09/BP01, in the Inverian zone at Badcall Point, and a core from statically retrogressed sample JM09/DP01 at Duartmore Point) indicate those zircon domains may have formed their current REE profile in the presence of a

metamorphic mineral that sequesters the HREE such as garnet. However, garnet has not been documented in the TTG gneisses of the Assynt Terrane, and is not stable in compositionally similar tonalites at pressures less than 15 kbar (Knudsen and Andersen, 1999); this pressure is greater than almost all of the peak pressures calculated in the Assynt Terrane and significantly higher than the most recent reliable estimate (Johnson and White, 2011).

The prevalence of relatively low Yb/Gd ratios and relatively flat chondrite-normalised heavy REE profiles in zircons from the metasedimentary rocks at Sithean Mor (samples JM08/22 and JM08/23) suggests that REE abundance in these zircons has been affected by garnet. Garnet is present in sample JM08/22, and although it was not found in sample JM08/23, it is widely distributed at this locality. The zircon REE link with garnet has the potential to allow zircon CL zones to be correlated with the tectonothermal evolution of the Assynt Terrane (Rubatto, 2002; Whitehouse and Platt, 2003). Petrological inspection and phase equilibria modelling by Zirkler et al. (2012) showed that garnet in similar metasedimentary rocks from elsewhere in the Assynt Terrane was present in both Badcallian and Inverian assemblages. This suggests that the zircon CL zones from Sithean Mor with relatively flat heavy REE profiles re-equilibrated in the presence of garnet during the either the Badcallian or Inverian tectonothermal events. The temperature estimates of Zirkler et al. (2012) for Inverian metamorphism (520–550 °C) are considered too low for zircon to equilibrate with its surrounding minerals, therefore the zircon rims with flat heavy REE profiles from Sithean Mor are suggested to have formed in the Badcallian tectonothermal event. Partial melting of these metasedimentary rocks in the Badcallian (Johnson et al., 2012, 2013; Rollinson, 2012; Rollinson and Gravestock, 2012) is also likely to have led to zircon rim growth from anatectic melt.

4.2. U-Th-Pb

Through zircon dating, this study sought to determine the age of TTG protolith formation of the Assynt Terrane and to attempt to distinguish ages for the Badcallian and Inverian metamorphic events. Our hypothesis was that zircons would yield ages reflecting the tectonothermal histories of their host samples (i.e. inside and outside Laxfordian shear zones, layered gneisses preserving Badcallian granulite-facies assemblages or statically retrogressed in the Inverian and/or Laxfordian). However, the ~500 Myr spread of concordant SIMS ages obtained did not correlate with sample tectonothermal history (Fig. 6). In order to obtain a protolith age for the TTG gneisses of the Assynt Terrane, a starting point is to look for the oldest age in the zircon populations from Badcall Point and Duartmore Point. The oldest age is 3017 ± 56 Ma, although this age is reversely discordant by 6%. This degree of reverse discordance is interpreted to be beyond the level of an analytical artefact affecting the U/Pb ratio calibration so this particular age may be overestimated. An alternative approach used by Whitehouse and Kemp (2010) to determine a protolith age is to assume that there is a single magmatic age and that the spread of ages has been caused by later Pb-loss. Successive rejection of the youngest ages is performed until the mean square of weighted deviates (MSWD) of the weighted average age of the population falls below a limit, below which analytical error can account for the observed scatter. This objective approach does not take account of the CL zoning pattern. The oldest age in the TTG gneiss zircon population is from a rim which is unlikely to reflect protolith formation whereas cores are much more likely to reflect the early stages of zircon history, possibly growth from a protolith magma (Corfu et al., 2003). Taking the threshold MSWD to be 1 (Whitehouse and Kemp, 2010), the oldest three cores yield a mean age of 2958 ± 7 Ma (MSWD = 1.00, probability = 0.37). Including the next youngest core increases the MSWD to only 1.3 which is still acceptable and yields a mean age of 2957 ± 14 Ma. These four oldest cores are all oscillatory zoned and thus are likely to have formed by crystallisation from a magma (Corfu et al., 2003). Cores with younger ages do not all show oscillatory zoning, and also greatly increase the MSWD. This age of 2957 ± 14 Ma is within error of the 2960 Ma age suggested by Friend and Kinny (1995) for the formation of the protolith to the Assynt Terrane. However, it is ~100 Myr older than the protolith age suggested by Whitehouse and Kemp (2010) and Crowley et al. (2014) who interpret that ages >~2850 Ma are inherited from an older magma.

Attempts to pick out ages for the Badcallian and Inverian metamorphic events from the zircon population in this study are hampered by the spread of concordant ages. In this study, no clustering of ages was found in any sample (Fig. 6a) or CL zoning pattern category (Fig. 6b). The fact that not all of the oldest ages in the population are from cores as might be expected, coupled with the spread of concordant ages of ~500 Myr in the different CL zoning pattern categories, makes interpretation of the chronological history of the Assynt Terrane extremely difficult. The youngest age in this population (2384 ± 46 Ma) is from a zircon rim from sample JM09/BP06 but is 46 Myr younger than the next youngest age and is reversely discordant by 2%. Adopting the approach used above to determine a protolith formation age, but rejecting the oldest ages until a MSWD threshold is reached, the youngest ten ages (those <2500 Ma) yield a mean age of 2479 ± 12 Ma (MSWD = 3.1, probability 0.001). As more ages are excluded, the MSWD only increases but by rejecting the 2384 ± 46 Ma and taking the next nine youngest ages, the MSWD drops to 1.3. Only by rejecting the second youngest age (2430 ± 44 Ma) as well, however, does the MSWD drop below 1 – the next eight youngest ages (ranging from 2459 ± 46 Ma to 2494 ± 28 Ma) yield a mean age of 2482 ± 6 Ma (MSWD = 0.69, probability = 0.68). This is considered to represent the age of a high-grade metamorphic event in the Assynt Terrane, as recognised by Friend and Kinny (1995) and Whitehouse and Kemp (2010). However, even our exhaustive study of the characteristics of individual zircon grains does not allow us to confirm whether this high-grade metamorphic event was at granulite facies (Badcallian) or amphibolite facies (Inverian).

Friend and Kinny (1995) also interpreted that a high-grade metamorphic event occurred at ~2500 Ma, the younger end of their spread of concordant SIMS data, which heterogeneously reset the zircon U-Pb systematics causing the spread of ages. They suggested this high grade event was the Badcallian, thus making it ~200 Myr younger than previously thought (Corfu et al., 1994). Whitehouse and Kemp (2010) agreed that there must have been a high-grade event at ~2500 Ma but could not disprove the idea that there was another high grade event at ~2700 Ma, something not considered by Friend and Kinny (1995). Using an incremental CA-ID-TIMS approach, Crowley et al. (2014) were able to distinguish age clusters at ~2700 Ma and ~2500 Ma, which they interpreted as pertaining to the Badcallian and Inverian respectively. Goodenough et al. (2013) obtained an age of ~2480 Ma from zircons from microgranite sheets with field relationships suggesting they were formed in the Inverian tectonothermal event. While the SIMS approach does not appear able to resolve a tectonothermal event at ~2700 Ma, our age of 2482 ± 6 Ma from the TTG gneisses is very close to that of Goodenough et al. (2013) obtained from granite sheets which suggests this age represents a high-grade tectonothermal event, possibly the Inverian. It is also possible that the high grade metamorphism followed by slow cooling (Johnson and White, 2011) has allowed intragrain Pb diffusion which has obscured the age of the Badcallian event. Further investigation of the process of Pb remobilisation may shed further light on this.

Dating of zircons from the metasedimentary rocks at Sithean Mor allows the possibility of constraining the timing of their deposition. When using zircons to constrain the depositional ages of

metasedimentary rocks, the youngest core age (interpreted to be detrital) is the maximum depositional age while the oldest rim age (interpreted to be metamorphic) is the minimum depositional age. At Sithean Mor, the youngest core age is 2506 ± 18 Ma and the oldest rim age is 2726 ± 28 Ma. This reversal of the expected pattern – metamorphic rims giving older ages than magmatic cores – indicates that the zircons from the metasedimentary rocks have had their Pb isotope systematics reset as well as those in the TTG gneisses. As a result, it is not possible to constrain the timing of deposition of the metasedimentary rocks at Sithean Mor. Goodenough et al. (2013) had a similar outcome from their attempts to date zircons from a different outcrop of metasedimentary rocks elsewhere in the Assynt Terrane.

REE profiling can enable zircon U-Pb ages to be linked to major metamorphic indicator minerals in the host rocks (e.g. Rubatto, 2002; Whitehouse and Platt, 2003; Kelly and Harley, 2005; Harley and Kelly, 2007). However, the TTG gneisses in this study showed limited variation in their REE profiles (Fig. 6) and together with the resetting of Pb isotope systematics this made it difficult to link ages to metamorphic minerals. In the metasedimentary rocks, low Yb/Gd ratios indicated that zircon had re-equilibrated in the presence of garnet, or a garnet-bearing partial melt, likely during partial melting in the Badcallian (Zirkler et al., 2012) but this occurred in all CL zoning categories, not just metamorphic rims as would be expected.

Ultimately, it is difficult to confidently assign zircon U-Pb ages from this study to magmatic or metamorphic events due to the resetting of Pb isotope systematics. Friend and Kinny (1995) and Whitehouse and Kemp (2010) referred to major and heterogeneous Pb-loss but the mechanism behind this phenomenon is elusive. MacDonald et al. (2013) conducted Electron Backscatter Diffraction analysis on the zircon population in this study; they found that very few zircons had lattice distortion which can facilitate element movement and those that did were not included in this study. Metamict zircons were not analysed in this study.

Although several metamorphic events can be recognised in the Assynt terrane of the Lewisian Gneiss Complex on the basis of field evidence, it is evident from our dataset – and from that of Whitehouse and Kemp (2010) – that these events cannot be recognised in the zircon age systematics of the TTG gneisses through SIMS analysis. Recent work by Crowley et al. (2014) using TIMS rather than SIMS was able to distinguish age populations, which were attributed to the Badcallian and Inverian events. However, the phase equilibria modelling of Zirkler et al. (2012) gave a temperature estimate of only 520–550 °C for the Inverian, although they acknowledge this may not be the peak temperature. This is still well below temperatures (>~750–800 °C) considered to enable zircon to equilibrate with its surroundings (e.g. Hoskin and Schaltegger, 2003) suggesting the Inverian event may have been too cold to be recorded in zircon systematics. While Friend and Kinny (1995) favoured an age of ~2500 Ma for the granulite-facies Badcallian tectonothermal event, Crowley et al. (2014) indisputably showed evidence for a major event recorded in zircon U-Pb systematics at ~2700 Ma. Field evidence for two granulite-facies events is not present but Whitehouse and Kemp (2010) also suggested this as a possibility. Direct dating of metamorphic minerals or magmatic rocks that can be linked directly to tectonothermal events may in future provide definitive ages.

4.3. Ti-in-zircon thermometry

Several previous studies have attempted to constrain the thermal history of the Assynt Terrane using a variety of palaeothermometers (e.g. O'Hara and Yarwood, 1978; Savage and Sills, 1980; Barnicoat, 1987; Sills and Rollinson, 1987). In this study, we apply the relatively new Ti-in-zircon thermometer (Watson et al., 2006). SIMS spot measurement of Ti concentration in zircon offers the possibility of determining the crystallisation temperature of magmatic cores and metamorphic rims, and therefore potentially the temperatures of the Lewisian protolith formation and subsequent metamorphic events. Ti content in zircon is proportional to the crystallisation temperature – this forms the basis of the Ti-in-zircon geothermometer derived by Watson et al. (2006). As the metamorphic conditions of the Inverian (520–550 °C, although potentially not peak temperature (Zirkler et al., 2012)) and Laxfordian (510–660 °C (Droop et al., 1999)) tectonothermal events are too low to be recorded in zircon trace element chemistry (e.g. Hoskin and Schaltegger, 2003), it is considered here that Ti-in-zircon thermometry will record minimum temperatures of the TTG protolith crystallisation and/or Badcallian metamorphism.

The accuracy of the temperatures calculated with the Ti-in-zircon thermometer is controlled by a_{TiO_2} – the presence of rutile in the rock indicates that $a_{TiO_2} = 1$ and Ti content in zircon formed with the rutile is buffered. In this situation, the calculated temperatures will be accurate. However, Ferry and Watson (2007) calibrated the thermometer equation to take into account subunity a_{TiO_2}; the lowest temperatures are calculated if zircon is assumed to be in equilibrium with rutile ($a_{TiO_2} = 1$) while temperature increases as a_{TiO_2} decreases. If there is no rutile present during zircon crystallisation, the system is not buffered and the calculated temperature will be a minimum. Rutile has been reported in felsic intrusive sheets (Rollinson, 1979, 1980) and some metasedimentary rocks (e.g. Zirkler et al., 2012) in the Assynt Terrane, but these rock compositions have not been studied in this contribution. Only sample JM09/SM09 (typical pristine Badcallian granulite-facies gneiss with granoblastic texture and an opx + cpx + plag + qtz assemblage) has rutile in its mineral assemblage, allowing the assumption of $a_{TiO_2} = 1$ during metamorphic zircon equilibration. As all the other samples in this study lack rutile the calculated zircon-Ti temperatures are minima.

In the TTG gneisses, the calculated minimum temperature range is 710–834 °C but the majority are ~780–800 °C (Table 4 and Fig. 7). There is no clear distinction in minimum temperature between magmatic cores and metamorphic rims (Fig. 7). This could be explained in three ways: (1) Ti distribution between cores and rims was unaffected by the Badcallian metamorphism; (2) magmatic crystallisation temperatures from zircon cores were overprinted during Badcallian metamorphism, or (3) cores represent minimum magmatic crystallisation temperatures and rims represent Badcallian metamorphic temperatures. The first scenario is unlikely as zircon rims are interpreted to have grown from anatectic melt during the Badcallian and so should record minimum Badcallian temperatures. The second scenario is also unlikely as fine CL zoning is preserved in many magmatic cores; Cherniak and Watson (2007) showed that higher temperatures and longer timescales are required to initiate diffusion of Ti than REEs such as Dy which precludes this hypothesis. We therefore interpret that despite the overlapping temperature ranges the cores represent minimum magmatic crystallisation temperatures (710–834 °C) and rims represent minimum Badcallian metamorphic temperatures (769–841 °C). The fact that core-rim textures are preserved in CL indicates temperature–time conditions were not sufficient to remobilise CL-controlling REEs. As remobilisation of Ti requires higher temperatures and longer timescales (Cherniak and Watson, 2007), the Ti in the zircon cores is interpreted not to have been remobilised and therefore still records minimum protolith crystallisation temperatures. Typical modern tonalites crystallise over a wide temperature range of ~700–1100 °C (e.g. Lambert and Wyllie, 1974; Shimura et al., 1992; Ishihara, 2005; Harrison et al., 2007) so the temperatures from cores fall within this range. The recent peak Badcallian temperature estimate by Johnson and White (2011) of 875–975 °C based on phase equilibria modelling of granulite-facies

Table 4
Ti-in-zircon minimum temperatures calculated using the thermometer of Watson et al. (2006). CL zoning pattern identifiers as Table 2.

Sample/spot	CL zoning pattern	Ti (ppm)	T (°C) at $a_{TiO_2} = 1$	2σ
JM09/BP02				
GMBP02Z1-1	h	15.43	788	28
GMBP02Z1-2	h	15.90	791	28
GMBP02Z2-1	ir	17.75	803	30
GMBP02Z2-2	ir	16.89	798	29
JM09/BP02 average			795	29
JM09/BP01				
BP01Z1-1	ir	18.66	808	30
GMBP01Z2-1	ir	14.53	782	27
JM09/BP01 average			795	29
JM09/BP06				
BP06ChZ1-1	r (br)	17.13	799	29
BP06ChZ1-2	c (ozp)	14.64	783	27
BP06ChZ2-1	c (ozp)	15.84	791	28
BP06ChZ2-2	c (ozp)	14.53	782	27
BP06ChZ2-3	c (ozp)	18.16	805	30
BP06ChZ2-6	r (dr)	19.42	812	31
BP06ChZ2-7	ir (emb)	12.15	765	26
BP06ChZ2-9	r (dr)	17.58	802	30
BP06Z3-1	ir	12.61	768	26
BP06Z3-2	ir	16.84	797	29
BP06Z3-3	ir	10.52	751	24
BP06Z3-4	ir	14.23	780	27
BP06Z3-5	ir	14.81	784	28
GMBP06Z1-1	r (br)	18.62	808	30
GMBP06Z1-2	r (br)	17.87	804	30
GMBP06Z1-3	c (bc)	15.66	790	28
GMBP06Z2-1	ir (emb)	16.72	797	29
GMBP06Z2-2	c (ozp)	18.75	809	30
GMBP06Z3-1	r (br)	15.39	788	28
GMBP06Z3-2	r (br)	14.84	784	28
GMBP06Z3-3	c (dc)	16.38	794	29
GMBP06Z4-1	r	15.00	785	28
GMBP06Z4-2	c (bc)	15.78	791	28
GMBP06Z4-3	c (bc)	13.78	777	27
GMBP06Z4-4	r	14.48	782	27
GMBP06Z5-1	r (br)	15.83	791	28
GMBP06Z5-2	c (dc)	14.60	783	27
GMBP06Z6-1	ir	23.72	834	33
JM09/BP06 average			791	28
JM09/BP04				
GMBP04Z1-1	r (br)	17.26	800	29
GMBP04Z1-2	r (br)	18.30	806	30
GMBP04Z2-1	r (br)	16.95	798	29
GMBP04Z2-2	r (br)	11.89	762	25
GMBP04Z3-1	c (bc)	16.13	793	29
GMBP04Z3-2	c (bc)	16.25	794	29
GMBP04Z4-1	r (br)	13.81	777	27
GMBP04Z4-2	r (br)	14.81	784	28
GMBP04Z4-3	c (dc)	8.58	732	22
GMBP04Z5-1	h	17.10	799	29
GMBP04Z5-2	h	17.30	800	29
GMBP04Z6-1	r (br)	18.91	809	30
GMBP04Z6-2	c (ozp)	19.13	811	31
GMBP04Z7-1	h	21.06	821	32
GMBP04Z7-2	h	18.59	808	30
GMBP04Z7-3	h	20.74	819	32
GMBP04Z8-2	h	19.12	811	31
GMBP04Z8-3	h	16.61	796	29
GMBP04Z9-1	h	16.60	796	29
GMBP04Z9-2	h	14.82	784	28
JM09/BP04 average			795	29
JM09/DP03				
GMDP03Z1-1	r (br)	13.09	772	26
GMDP03Z1-2	r (br)	12.66	769	26
GMDP03Z1-3	c (ozp)	6.71	710	20
GMDP03Z1-4	r (br)	14.07	779	27
GMDP03Z1-5	r (br)	13.03	771	26
GMDP03Z2-1	c (ozp)	19.64	813	31
DP03Z2-1	h	19.41	812	31
JM09/DP03 average			775	27

Table 4 (*Continued*)

Sample/spot	CL zoning pattern	Ti (ppm)	T (°C) at $a_{TiO_2} = 1$	2σ
JM09/DP01				
DP01Z4-1	h	17.78	803	30
DP01Z4-2	h	16.39	794	29
DP01Z6-1	r (br)	17.14	799	29
DP01Z6-2	r (br)	15.90	791	28
DP01Z6-3	c (dc)	15.09	786	28
DP01Z6-4	r (br)	17.78	803	30
DP01Z6-5	r (br)	18.59	808	30
DP01Z10-1	r (br)	20.28	817	31
DP01Z10-2	r (br)	19.81	814	31
GMDP01Z2-2	c (dc)	14.87	785	28
GMDP01Z2-4	c (dc)	14.15	780	27
GMDP01Z2-5	r (br)	15.15	786	28
GMDP01Z3-1	h	20.75	819	32
GMDP01Z4-1	h	9.95	745	24
GMDP01Z4-2	h	12.78	769	26
GMDP01Z5-1	c (dc)	10.81	753	24
GMDP01Z5-2	r (br)	17.20	800	29
GMDP01Z6-1	r (br)	13.70	776	27
GMDP01Z6-2	r (br)	14.19	780	27
GMDP01Z6-3	c (dc)	13.87	778	27
GMDP01Z7-1	h	19.31	812	31
GMDP01Z8-1	r (br)	15.34	788	28
GMDP01Z9-3	ir	13.42	774	27
JM09/DP01 average			787	28
Average all TTG			790	
JM08/22				
GM22Z1-1	c (ozp)	21.31	822	32
GM22Z1-2	c (bc)	19.97	815	31
GM22Z2-1	c (ozp)	22.97	830	33
GM22Z3-1	c (ozp)	19.39	812	31
GM22Z4-1	ir	19.84	815	31
JM08/22 average			819	32
JM08/23				
GM23Z1-1	ir	17.80	803	30
GM23Z2-1	ir	19.54	813	31
GM23Z2-2	ir	24.39	837	34
GM23Z4-1	r (br)	24.32	837	34
GM23Z4-2	r (br)	25.19	841	34
GM23Z5-1	h	20.55	818	31
GM23Z5-2	h	17.94	804	30
GM23Z6-1	ir	26.69	847	35
GM23Z6-2	ir	22.06	826	32
GM23Z6-3	ir	24.48	838	34
JM08/23 average			826	32
Average all metasediments			823	

assemblages in mafic gneiss is higher than the range of Ti temperatures from metamorphic rims but as these Ti-temperatures are minima, the results are at least consistent with granulite metamorphic conditions. In addition, Roberts and Finger (1997) showed that zircon would grow or recrystallize after peak metamorphism in granulite-facies gneiss. The fact that the zircon temperatures in this study are slightly lower than the peak metamorphic assemblage temperatures calculated by Johnson and White (2011) is in accord with this phenomenon. This suggests that the Ti-in-zircon thermometer could be recording a post-peak Badcallian temperature.

Zircon from the metasedimentary rocks at Sithean Mor records higher Ti-in-zircon temperatures than from the TTG gneisses from Badcall Point and Duartmore Point. At $a_{TiO_2} = 1$, the average temperature is 823 °C compared to 790 °C in the TTG gneisses and the minimum recorded temperature from Sithean Mor of 803 °C is much higher than the lowest from the TTG gneisses (710 °C) (Table 4 and Fig. 7). Cores with magmatic CL patterns are interpreted to be detrital and have an average minimum temperature of 820 °C, higher than magmatic cores from the TTG gneisses. As the metasedimentary rocks are interpreted to predate the TTG gneisses (Rollinson and Gravestock, 2012), this temperature is tentatively interpreted to represent zircon crystallisation in a pre-Lewisian rock. The two zircons with convincing metamorphic rims yield an average temperature of 839 °C, lower than the temperature estimate of Johnson and White (2011) for peak Badcallian metamorphism but at least consistent with granulite conditions for zircon rim equilibration. The higher minimum temperature for Badcallian metamorphism calculated from these zircons relative to those in the TTG gneisses is interpreted to reflect greater availability of Ti.

4.4. Overall history of the Assynt Terrane

This contribution has sought to determine the chronological and thermal histories of the Assynt Terrane of the Lewisian Gneiss Complex. A single study cannot provide a complete picture of this and so in this section we place our results in the context of previous work to construct an overall temperature–time history of the Assynt Terrane during Archaean to Palaeoproterozoic times (Table 5). A key remaining issue in the history of the Assynt Terrane is the absolute age of the Badcallian tectonothermal event. Initial U-Pb zircon

Table 5
Summary table of the temperature-time history of the Assynt Terrane combining data from this study and previously published work.

Event	Timing	Temperature
TTG protolith formation	2958 ± 7 Ma (this study), 2960–3030 Ma (Friend and Kinny, 1995), ~2843 Ma (Goodenough et al., 2013), ~2850 Ma (Whitehouse and Kemp, 2010), all from U-Pb zircon dating	Minimum 710–834 °C (this study) from Ti-in-zircon thermometry
Badcallian tectonothermal event	2482 ± 6 Ma (this study), ~2500 Ma (Friend and Kinny, 1995) or ~2700 Ma (Corfu et al., 1994; Whitehouse and Kemp, 2010; Crowley et al., 2014), all from TTG gneisses), all from U-Pb zircon dating	Minimum 769–841 °C (this study) from Ti-in-zircon thermometry, ~875–975 °C (Johnson and White, 2011) from TTG gneisses, >900 °C (Zirkler et al., 2012) from metasedimentary rocks, both from mineral equilibria modelling
Inverian tectonothermal event	2482 ± 6 Ma (this study), ~2480 Ma (Corfu et al., 1994; Goodenough et al., 2013) from microgranite sheets/pegmatite, ~2500 Ma (Corfu et al., 1994; Whitehouse and Kemp, 2010; Crowley et al., 2014) from TTG gneisses, all from U-Pb zircon dating	~520–550 °C (Zirkler et al., 2012) from mineral equilibria modelling of metasedimentary rocks but not necessarily peak metamorphism, ~600 °C (Sills, 1983) from ion-exchange thermometers on TTG gneisses
Intrusion of Scourie Dyke Swarm	~2418–2375 Ma (Davies and Heaman, 2014) from U-Pb dating of zircon and baddeleyite	No absolute estimates
Arc magmatism	~1880 Ma (Goodenough et al., 2013) from U-Pb zircon dating of alkaline granites	No absolute estimates
Laxfordian tectonothermal event	~1790–1670 Ma (Corfu et al., 1994; Kinny et al., 2005), from U-Pb dating of zircon and titanite in TTG gneisses	~530–630 °C (Droop et al., 1999) from ion exchange thermometry on the Loch Maree Group in southern LGC (not in Assynt Terrane)

dating by Corfu et al. (1994) suggested it occurred at ~2710 Ma but ion microprobe dating by Friend and Kinny (1995) led them to interpret it occurred at ~2500 Ma. A novel approach of sequential CA-ID-TIMS zircon U-Pb dating by Crowley et al. (2014) has recently indicated there is a high-grade metamorphic event at ~2700 Ma which they have attributed to the Badcallian. Furthermore, an age of ~2480 Ma was obtained for microgranite sheets with field relationships indicating they were formed in the Inverian tectonothermal event (Goodenough et al., 2013). Similarly, Corfu et al. (1994) dated a pegmatite cross-cut by a Scourie Dyke at ~2480 Ma. This would suggest that the ~2500 Ma age from the TTG gneisses interpreted by Friend and Kinny (1995) to be the Badcallian is actually the Inverian. However, it should be noted that the temperature estimate from a mineral assemblage interpreted to be Inverian in age by Zirkler et al. (2012) of 520–550 °C is well below the closure temperature of the U-Pb system in zircon (Cherniak and Watson, 2001). It is therefore possible that a second high-grade, potentially granulite-facies, tectonothermal event occurred at ~2500 Ma, although there is no field evidence for this. Alternatively, the mineral assemblage analysed by Zirkler et al. (2012) may not in fact be peak-Inverian. It seems likely that the most effective way to date the Badcallian event will be to date magmatic rocks that are clearly associated with this event, rather than attempting further to identify metamorphic ages in the complex TTG gneisses.

5. Conclusions

Zircons from a range of TTG gneisses and metasedimentary rocks from the Assynt Terrane, a significant part of the Precambrian Lewisian Gneiss Complex of Northwest Scotland, have been analysed for U-Th-Pb and Ti, with the intention of constraining the temperature-time history. This contribution has presented the first application of Ti-in-zircon thermometry (Watson et al., 2006) to the Lewisian. Furthermore, analysis of these trace elements and isotopes in the context of field and petrographic characterisation and zircon cathodoluminescence imaging/REE profiling of internal chemical zoning has raised the following key points about the history of the Assynt Terrane:

- The oldest three cores yield a mean age of 2958 ± 7 Ma (MSWD = 1.00, probability = 0.37). This is older than the magmatic protolith ages interpreted by Whitehouse and Kemp (2010) and Crowley et al. (2014) but is close to that derived by Friend and Kinny (1995) for the formation of the protolith to the Assynt Terrane.
- A high-grade tectonothermal event occurred at 2482 ± 6 Ma. This age is very close to the age of 2480 Ma obtained by Goodenough et al. (2013) from granite sheets that have field relationships indicating they are Inverian in age. However, the best available temperature estimate for the Inverian tectonothermal event (520–550 °C (Zirkler et al., 2012)) is below the temperature at which zircon trace element systems are likely to be reset. We recognise a spread of concordant ages from the protolith crystallisation age of 2958 ± 7 Ma to 2482 ± 6 Ma, which are likely to encompass the Badcallian and Inverian metamorphic events. It remains possible that there were two granulite-facies tectonothermal events at ~2700 Ma and ~2500 Ma. It is clear that resolving the ages of these events by SIMS is difficult within these complex zircon systematics (as recognised by Whitehouse and Kemp (2010)), but identification of associated magmatism or novel approaches such as that of Crowley et al. (2014) will lead to this.
- Zircons in the metasedimentary rocks have relatively flat chondrite-normalised heavy REE profiles (low Yb/Gd ratios), which suggest they equilibrated with Badcallian metamorphic garnet. However, a range of U-Pb ages are recorded in these zircons and therefore a definitive age for the Badcallian cannot be determined from these zircons.
- Ti-in-zircon thermometry (Watson et al., 2006) records temperatures of 710–834 °C for zircon cores in the TTG gneisses, interpreted to record the minimum crystallisation temperature of the magmatic protolith. Zircon rims record minimum temperatures of 769–841 °C, interpreted to represent minimum temperatures for Badcallian metamorphism and post-peak Badcallian anatectic zircon growth.
- Zircons in the metasedimentary rocks record generally higher minimum temperatures, with an average of 823 °C compared to 790 °C in the TTG gneisses. The zircon cores in the metasedimentary rocks are interpreted to be detrital and the calculated temperatures are interpreted to record zircon crystallisation in a magmatic protolith that predates the Lewisian Gneiss Complex. Zircon rims record temperatures that are lower than the estimates of Johnson and White (2011) for peak Badcallian metamorphism but are consistent with metamorphism of the sediments under granulite facies conditions in that event.

Acknowledgements

This work was carried out under UK Natural Environment Research Council DTG NE/G523855/1 and British Geological Survey CASE Studentship 2K08E010 to JMM. Richard Holme assisted with thermometry calculations. Ion microprobe analysis at the Edinburgh Ion Microprobe Facility was carried out with funding from NERC grant IMF384/1109; Richard Hinton, Cees-Jan De Hoog and John Craven are thanked for ion microprobe support and Mike Hall for assistance with sample preparation. KMG publishes with the permission of the Executive Director of the Geological Survey. Tim Johnson and Hugh Rollinson are thanked for their thorough reviews of this manuscript.

References

Attfield, P., 1987. The structural history of the Canisp shear zone. In: Park, R.G., Tarney, J. (Eds.), Evolution of the Lewisian and Comparable Precambrian High-Grade Terrains.

Barnicoat, A.C., 1983. Metamorphism of the Scourian complex, NW Scotland. J. Metamorph. Geol. 1, 163–182.

Barnicoat, A.C., 1987. The causes of high-grade metamorphism of the Scourie complex, NW Scotland. In: Park, R.G., Tarney, J. (Eds.), Evolution of the Lewisian and Comparable Precambrian High-Grade Terrains. Blackwells.

Bea, F., Montero, P., 1999. Behavior of accessory phases and redistribution of Zr, REE, Y, Th, and U during metamorphism and partial melting of metapelites in the lower crust: an example from the Kinzigite Formation of Ivrea-Verbano, NW Italy. Geochim. Cosmochim. Acta 63 (7–8), 1133–1153.

Bea, F., Pereira, M.D., Stroh, A., 1994. Mineral/leucosome trace-element partitioning in a peraluminous migmatite (a laser ablation-ICP-MS study). Chem. Geol. 117 (1–4), 291–312.

Beach, A., 1973. Mineralogy of high-temperature shear zones at Scourie, NW Scotland. J. Petrol. 14 (2), 231–248.

Cartwright, I., Barnicoat, A.C., 1987. Petrology of Scourian supracrustal rocks and orthogneisses from Stoer, NW Scotland: implications for the geological evolution of the Lewisian complex. In: Park, R.G., Tarney, J. (Eds.), Evolution of the Lewisian and Comparable Precambrian High-Grade Terrains. Blackwells.

Cartwright, I., Fitches, W.R., O' Hara, M.J., Barnicoat, A.C., O' Hara, S., 1985. Archaean supracrustal rocks from the Lewisian near Stoer, Sutherland. Scot. J. Geol. 21 (2), 187–196.

Cherniak, D.J., Watson, E.B., 2001. Pb diffusion in zircon. Chem. Geol. 172 (1–2), 5–24.

Cherniak, D.J., Watson, E.B., 2007. Ti diffusion in zircon. Chem. Geol. 242 (3–4), 473–483.

Corfu, F., Hanchar, J.M., Hoskin, P.W.O., Kinny, P.D., 2003. Atlas of zircon textures. In: Hanchar, J.M., Hoskin, P.W.O. (Eds.), Zircon, vol. 53. Mineralogical Society of America and the Geochemical Society.

Corfu, F., Heaman, L.M., Rogers, G., 1994. Polymetamorphic evolution of the Lewisian Complex, NW Scotland, as recorded by U-Pb isotopic compositions of zircon, titanite and rutile. Contrib. Mineral. Petrol. 117 (3), 215–228.

Crowley, Q.G., Key, R., Noble, S.R., 2014. High-precision U–Pb dating of complex zircon from the Lewisian Gneiss Complex of Scotland using an incremental CA-ID-TIMS approach. Gondwana Res. (in press).

Davidson, J., Turner, S., Handley, H., Macpherson, C., Dosseto, A., 2007. Amphibole "sponge" in arc crust? Geology 35 (9), 787–790.

Davies, F.B., 1974. A layered basic complex in the Lewisian south of Loch Laxford, Sutherland. J. Geol. Soc. 130, 279–284.

Davies, J.H.F.L., Heaman, L., 2014. New U-Pb baddeleyite and zircon ages for the Scourie dyke swarm: a long-lived large igneous province with implications for the Paleoproterozoic evolution of NW Scotland. Precambrian Res. 249, 180–198.

Droop, G.T.R., Fernandes, L.A.D., Shaw, S., 1999. Laxfordian metamorphic conditions of the Palaeoproterozoic Loch Maree Group, Lewisian Complex, NW Scotland. Scot. J. Geol. 35, 31–50.

Evans, C.R., 1965. Geochronology of the Lewisian Basement near Lochinver, Sutherland. Nature 204, 638–641.

Ferry, J.M., Watson, E.B., 2007. New thermodynamic models and revised calibrations for the Ti-in-zircon and Zr-in-rutile thermometers. Contrib. Mineral. Petrol. 154 (4), 429–437.

Friend, C.R.L., Kinny, P.D., 1995. New evidence for protolith ages of Lewisian granulites, Northwest Scotland. Geology 23 (11), 1027–1030.

Friend, C.R.L., Kinny, P.D., 2001. A reappraisal of the Lewisian Gneiss Complex: geochronological evidence for its tectonic assembly from disparate terranes in the Proterozoic. Contrib. Mineral. Petrol. 142 (2), 198–218.

Goodenough, K.M., Crowley, Q., Krabbendam, M., Parry, S.F., 2013. New U-Pb age constraints for the Laxford Shear Zone, NW Scotland: evidence for tectono-magmatic processes associated with the formation of a Palaeoproterozoic supercontinent. Precambrian Res. 223, 1–19.

Goodenough, K.M., Park, R.G., Krabbendam, M., Myers, J.S., Wheeler, J., Loughlin, S.C., Crowley, Q.G., Friend, C.R.L., Beach, A., Kinny, P.D., Graham, R.H., 2010. The Laxford Shear Zone: an end-Archaean terrane boundary? In: Law, R.D., Butler, R.W.H., Holdsworth, R.E., Krabbendam, M., Strachan, R.A. (Eds.), Continental Tectonics and Mountain Building, vol. 335. Geological Society, London.

Harley, S.L., Kelly, N.M., 2007. The impact of zircon-garnet REE distribution data on the interpretation of zircon U-Pb ages in complex high-grade terrains: an example from the Rauer Islands, East Antarctica. Chem. Geol. 241 (1–2), 62–87.

Harrison, T.M., Watson, E.B., Aikman, A.B., 2007. Temperature spectra of zircon crystallization in plutonic rocks. Geology 35 (7), 635–638.

Hinton, R.W., Upton, B.G.J., 1991. The chemistry of zircon: variations within and between large crystals from syenite and alkali basalt xenoliths. Geochim. Cosmochim. Acta 55 (11), 3287–3302.

Holland, T.J.B., Powell, R., 1998. An internally consistent thermodynamic data set for phases of petrological interest. J. Metamorph. Geol. 16 (3), 309–343.

Hoskin, P.W.O., 1998. Minor and trace element analysis of natural zircon (ZrSiO4) by SIMS and laser ablation ICPMS: a consideration and comparison of two broadly competitive techniques. J. Trace Microprobe Tech. 16 (3), 301–326.

Hoskin, P.W.O., Black, L.P., 2000. Metamorphic zircon formation by solid-state recrystallization of protolith igneous zircon. J. Metamorph. Geol. 18 (4), 423–439.

Hoskin, P.W.O., Ireland, T.R., 2000. Rare earth element chemistry of zircon and its use as a provenance indicator. Geology 28 (7), 627–630.

Hoskin, P.W.O., Schaltegger, U., 2003. The composition of zircon and igneous and metamorphic petrogenesis. In: Hanchar, J., Hoskin, P.W.O. (Eds.), Zircon, vol. 53. Mineralogical Society of America and the Geochemical Society, pp. 27–62.

Ishihara, S., 2005. Fifth Hutton Symposium: The Origin of Granites and Related Rocks: Proceedings of a Symposium , Toyohashi, Japan, 2–6 September 2003. Geological Society of America, p. 390.

Jensen, L.N., 1984. Quartz microfabric of the Laxfordian Canisp shear zone, NW Scotland. J. Struct. Geol. 6 (3), 293–302.

Johnson, T.E., Fischer, S., White, R.W., 2013. Field and petrographic evidence for partial melting of TTG gneisses from the central region of the mainland Lewisian complex, NW Scotland. J. Geol. Soc. 170 (2), 319–326.

Johnson, T.E., Fischer, S., White, R.W., Brown, M., Rollinson, H.R., 2012. Archaean intracrustal differentiation from partial melting of Metagabbro-field and geochemical evidence from the central region of the Lewisian Complex, NW Scotland. J. Petrol. 53 (10), 2115–2138.

Johnson, T.E., White, R.W., 2011. Phase equilibrium constraints on conditions of granulite-facies metamorphism at Scourie, NW Scotland. J. Geol. Soc. 168 (1), 147–158.

Kelly, N.M., Harley, S.L., 2005. An integrated microtextural and chemical approach to zircon geochronology: refining the Archaean history of the Napier Complex, east Antarctica. Contrib. Mineral. Petrol. 149 (1), 57–84.

Kelly, N.M., Hinton, R.W., Harley, S.L., Appleby, S.K., 2008. New SIMS U-Pb zircon ages from the Langavat Belt, South Harris, NW Scotland: implications for the Lewisian terrane model. J. Geol. Soc. 165, 967–981.

Kinny, P.D., Friend, C.R.L., 1997. U-Pb isotopic evidence for the accretion of different crustal blocks to form the Lewisian Complex of northwest Scotland. Contrib. Mineral. Petrol. 129, 326–340.

Kinny, P.D., Friend, C.R.L., Love, G.J., 2005. Proposal for a terrane-based nomenclature for the Lewisian Gneiss complex of NW Scotland. J. Geol. Soc. 162, 175–186.

Knudsen, T.L., Andersen, T., 1999. Petrology and geochemistry of the Tromoy gneiss complex, South Norway, an alleged example of Proterozoic depleted lower continental crust. J. Petrol. 40 (6), 909–933.

Lambert, I.B., Wyllie, P.J., 1974. Melting of tonalite and crystallisation of andesite liquid with excess water to 30 kilobars. J. Geol. 82 (1), 88–97.

Love, G.J., Friend, C.R.L., Kinny, P.D., 2010. Palaeoproterozoic terrane assembly in the Lewisian Gneiss complex on the Scottish mainland, south of Gruinard Bay: SHRIMP U-Pb zircon evidence. Precambrian Res. 183 (1), 89–111.

Love, G.J., Kinny, P.D., Friend, C.R.L., 2004. Timing of magmatism and metamorphism in the Gruinard Bay area of the Lewisian Gneiss complex: comparisons with the Assynt Terrane and implications for terrane accretion. Contrib. Mineral. Petrol. 146 (5), 620–636.

Ludwig, K.R., 2003. User's Manual for Isoplot 3.00: A Geochronological Toolkit for Excel. Berkeley Geochronological Center, Special Publications.

Maas, R., Kinny, P.D., Williams, I.S., Froude, D.O., Compston, W., 1992. The Earths Oldest Known crust – a geochronological and geochemical study of 3900–4200 Ma old detrital zircons from Mt Narryer and Jack Hills, Western-Australia. Geochim. Cosmochim. Acta 56 (3), 1281–1300.

MacDonald, J.M., Wheeler, J., Harley, S.L., Mariani, E., Goodenough, K.M., Crowley, Q., Tatham, D., 2013. Lattice distortion in a zircon population and its effects on trace element mobility and U–Th–Pb isotope systematics: examples from the Lewisian Gneiss Complex, northwest Scotland. Contrib. Mineral. Petrol. 166 (1), 21–41.

McDonough, W.F., Sun, S.s., 1995. The composition of the Earth. Chem. Geol. 120 (3–4), 223–253, http://dx.doi.org/10.1016/0009-2541(94)00140-4.

Murali, A.V., Parthasarathy, R., Mahadevan, T.M., Das, M.S., 1983. Trace-elements characteristics, REE patterns and partition-coefficients of zircons from different geological environments – a case-study on Indian zircons. Geochim. Cosmochim. Acta 47 (11), 2047–2052.

O' Hara, M.J., Yarwood, G., 1978. High pressure-temperature point on an Archaean Geotherm, implied magma genesis by crustal anatexis, and consequences for garnet-pyroxene thermometry and barometry. Philos. Trans. R. Soc. Lond. Ser. A: Math. Phys. Eng. Sci. 288 (1355), 441–453.

Okeke, P.O., Borley, G.D., Watson, J., 1983. A geochemical study of Lewisian meta-sedimentary granulites and gneisses in the Scourie-Laxford area of the Northwest Scotland. Mineral. Mag. 47 (342), 1–9.

Park, R.G., 1970. Observations on Lewisian chronology. Scot. J. Geol. 6 (4), 379–399.

Park, R.G., 2005. The Lewisian terrane model: a review. Scot. J. Geol. 41, 105–118.

Park, R.G., Kinny, P.D., Friend, C.R.L., Love, G.J., 2005. Discussion on a terrane-based nomenclature for the Lewisian Gneiss complex of NW Scotland. J. Geol. Soc. 162, 893–895.
Peach, B.N., Horne, J., Gunn, W., Clough, C.T., Hinxman, L.W., 1907. The Geological Structure of the Northwest Highlands of Scotland. H.M.S.O., Memoirs of the Geological Survey, London.
Roberts, M.P., Finger, F., 1997. Do U-Pb zircon ages from granulites reflect peak metamorphic conditions? Geology 25 (4), 319–322.
Rollinson, H., 1980. Iron-titanium oxides as an indicator of the role of the fluid phase during the cooling of granites metamorphosed to granulite grade. Mineral. Mag. 43, 623–631.
Rollinson, H., 2012. Geochemical constraints on the composition of Archaean lower continental crust: partial melting in the Lewisian granulites. Earth Planet. Sci. Lett. 351–352, 1–12.
Rollinson, H., Gravestock, P., 2012. The trace element geochemistry of clinopyroxenes from pyroxenites in the Lewisian of NW Scotland: insights into light rare earth element mobility during granulite-facies metamorphism. Contrib. Mineral. Petrol. 163, 319–335.
Rollinson, H.R., 1979. Ilmenite-magnetite geothermometry in Trondhjemites from the Scourian complex of NW Scotland. Mineral. Mag. 43 (325), 165–170.
Rubatto, D., 2002. Zircon trace element geochemistry: partitioning with garnet and the link between U-Pb ages and metamorphism. Chem. Geol. 184 (1–2), 123–138.
Rubatto, D., Hermann, J., 2006. Zircon/garnet trace element partitioning: a tool for P-T-time paths. Geochim. Cosmochim. Acta 70 (18), A542.
Rubatto, D., Williams, I.S., Buick, I.S., 2001. Zircon and monazite response to prograde metamorphism in the Reynolds Range, central Australia. Contrib. Mineral. Petrol. 140 (4), 458–468.
Savage, D., Sills, J.D., 1980. High-pressure metamorphism in the Scourian of NW Scotland – evidence from garnet granulites. Contrib. Mineral. Petrol. 74 (2), 153–163.
Schaltegger, U., Fanning, C.M., Gunther, D., Maurin, J.C., Schulmann, K., Gebauer, D., 1999. Growth, annealing and recrystallization of zircon and preservation of monazite in high-grade metamorphism: conventional and in-situ U-Pb isotope, cathodoluminescence and microchemical evidence. Contrib. Mineral. Petrol. 134 (2–3), 186–201.
Shimura, T., Komatsu, M., Iiyama, J.T., 1992. Genesis of the lower crustal garnet-orthopyroxene tonalites (S-type) of the Hidaka Metamorphic Belt, northern Japan. Trans. R. Soc. Edinburgh Earth Sci. 83, 259–268.
Sills, J.D., 1983. Mineralogical changes occurring during the retrogression of Archean gneisses from the Lewisian complex of NW Scotland. Lithos 16 (2), 113–124.
Sills, J.D., Rollinson, H.R., 1987. Metamorphic evolution of the mainland Lewisian complex. In: Park, R.G., Tarney, J. (Eds.), Evolution of the Lewisian and Comparable Precambrian High-Grade Terrains. Blackwells.
Slama, J., Kosler, J., Condon, D.J., Crowley, J.L., Gerdes, A., Hanchar, J.M., Horstwood, M.S.A., Morris, G.A., Nasdala, L., Norberg, N., Schaltegger, U., Schoene, B., Tubrett, M.N., Whitehouse, M.J., 2008. Plesovice zircon – a new natural reference material for U-Pb and Hf isotopic microanalysis. Chem. Geol. 249 (1–2), 1–35.
Sutton, J., Watson, J., 1951. The pre-Torridonian metamorphic history of the Loch Torridon and Scourie areas in the North-West Highlands, and its bearing on the chronological classification of the Lewisian. Quart. J. Geol. Soc. 106, 241–296.
Tarney, J., Weaver, B.L., 1987. Geochemistry of the Scourian complex: petrogenesis and tectonic models. In: Park, R.G., Tarney, J. (Eds.), Evolution of the Lewisian and Comparable Precambrian High-Grade Terrains. Blackwells.
Watson, E.B., Harrison, T.M., 2005. Zircon thermometer reveals minimum melting conditions on earliest Earth. Science 308 (5723), 841–844.
Watson, E.B., Wark, D.A., Thomas, J.B., 2006. Crystallization thermometers for zircon and rutile. Contrib. Mineral. Petrol. 151 (4), 413–433.
Wheeler, J., Park, R.G., Rollinson, H.R., Beach, A., 2010. The Lewisian complex: insights into deep crustal evolution. In: Law, R.D., Butler, R.W.H., Holdsworth, R.E., Krabbendam, M., Strachan, R.A. (Eds.), Continental Tectonics and Mountain Building, vol. 335. The Geological Society Publishing House.
Whitehouse, M., Kemp, A.I.S., 2010. On the difficulty of assigning crustal residence, magmatic protolith and metamorphic ages to Lewisian granulites: constraints from combined in-situ U-Pb and Lu-Hf isotopes. In: Law, R.D., Butler, R.W.H., Holdsworth, R.E., Krabbendam, M., Strachan, R.A. (Eds.), Continental Tectonics and Mountain Building: The Legacy of Peach and Horne, vol. 335. The Geological Society Publishing House.
Whitehouse, M.J., Kamber, B.S., 2003. A rare earth element study of complex zircons from early Archaean Amitsoq gneisses, Godthabsfjord, south-west Greenland. Precambrian Res. 126 (3–4), 363–377.
Whitehouse, M.J., Platt, J.P., 2003. Dating high-grade metamorphism – constraints from rare-earth elements in zircon and garnet. Contrib. Mineral. Petrol. 145 (1), 61–74.
Wiedenbeck, M., Allé, P., Corfu, F., Griffin, W.L., Meier, M., Oberli, F., Quadt, A.V., Roddick, J.C., Spiegel, W., 1995. Three natural zircon standards for U-Th-Pb, Lu-Hf, trace element and REE analyses. Geostandards Newslett. 19 (1), 1–23.
Zirkler, A., Johnson, T.E., White, R.W., Zack, T., 2012. Polymetamorphism in the mainland Lewisian complex, NW Scotland – phase equilibria and geochronological constraints from the Cnoc an t'Sidhean suite. J. Metamorph. Geol. 30 (8), 865–885.